New Parameterizations for Neutral and Ion-Induced Sulfuric Acid-Water Particle Formation in Nucleation and Kinetic Regimes

Määttänen, Anni

2018-01-27

Määttänen , A , Merikanto , J , Henschel , H , Duplissy , J , Makkonen , R , Ortega , I K & Vehkamäki , H 2018 , ' New Parameterizations for Neutral and Ion-Induced Sulfuric Acid-Water Particle Formation in Nucleation and Kinetic Regimes ' , Journal of Geophysical Research : Atmospheres , vol. 123 , no. 2 , pp. 1269-1296 . https://doi.org/10.1002/2017JD027429

http://hdl.handle.net/10138/233943
https://doi.org/10.1002/2017JD027429

unspecified
acceptedVersion

New parameterizations for neutral and ion-induced two-component sulfuric acid-water particle formation in nucleation and kinetic regimes

Anni Määttänen[1], Joonas Merikanto[2], Henning Henschel[3], Jonathan Duplissy[3], Ismael K. Ortega[4], Risto Makkonen[3]and Hanna Vehkamäki [3]

[1]LATMOS/IPSL, UVSQ Université Paris-Saclay, UPMC Univ. Paris 06, CNRS, 11 boulevard d'Alembert, 78280 Guyancourt, France.

[2]Finnish Meteorological Institute, Helsinki, Finland.

[3]Department of Physics, University of Helsinki, Helsinki, Finland.

[4]Onera-The French Aerospace Lab, F-91761 Palaiseau, France

Key Points:

- Improved particle formation parameterizations have been developed
- Both neutral and ion-induced pathways are considered and the kinetic regime is accounted for
- We recommend using these parameterizations from now on

Corresponding author: A. Määttänen, anni.maattanen@latmos.ipsl.fr

Abstract

We have developed new parameterizations of two-component neutral homogeneous and ion-induced sulfuric acid - water particle formation for large ranges of environmental conditions, based on an improved model that has been validated against Cosmics Leaving OUtdoor Droplets (CLOUD) experiments at CERN. The neutral parameterization is valid for the following ranges: temperatures 165-400 K, sulfuric acid concentrations 10^4-10^{13} cm^{-3} and relative humidities 0.001-100%. The ion-induced parameterization is valid for temperatures 195-400 K, sulfuric acid concentrations 10^4-10^{16} cm^{-3} and relative humidities 10^{-5}-100%. The new parameterizations are thus applicable for the full range of Earth's atmospheric conditions where binary sulfuric acid - water particle formation is relevant, including both tropospheric and stratospheric conditions. They can also be used for describing particle formation in the atmosphere of Venus. The model is based on a thermodynamically consistent version of Classical Nucleation Theory normalized using quantum chemical data. The model is also applicable to extreme dry conditions where the one-component sulfuric acid limit is approached. Parameterizations are presented for critical cluster sulfuric acid mole fraction, radius, total number of molecules, and particle formation rate. If the critical cluster contains only one sulfuric acid molecule, a simple formula for kinetic particle formation can be used: this threshold has also been parameterized.

1 Introduction

Aerosols affect Earth's climate by scattering solar radiation and acting as cloud condensation nuclei [*Boucher et al.*, 2013] and thus they significantly affect the radiation balance within the Earth's atmosphere. Sulfur is transmitted into the Earth's atmosphere as gaseous SO_2 and other gaseous sulfur species. These species are transformed into gaseous sulfuric acid through atmospheric oxidation. The gaseous sulfuric acid generates new atmospheric aerosol particles through secondary particle formation processes. Global aerosol models show that secondary particles formed in the atmosphere dominate the total global aerosol number concentrations and generate up to half of global cloud condensation nuclei (CCN)[*Spracklen et al.*, 2008; *Merikanto et al.*, 2009]. Observed particle formation rates are often proportional to the abundance of gaseous sulfuric acid [*Weber et al.*, 1996; *Sihto et al.*, 2006; *Kuang et al.*, 2008; *Petäjä et al.*, 2009], suggesting that sulfuric acid is a key compound in atmospheric new particle formation in the Earth's troposphere. However, in the lower troposphere also additional compounds are required to stabilize the sulfuric acid clusters [*Sipilä et al.*, 2010; *Zhao et al.*, 2010; *Petäjä et al.*, 2011] and

allow their growth to atmospherically relevant sizes [*Ortega et al.*, 2012]. However, in the upper troposphere pure sulfuric acid -water particle formation is likely an efficient mechanism for new particle formation [*Kirkby et al.*, 2011; *Merikanto et al.*, 2015]. A significant fraction of boundary layer CCN originate from particles formed in the upper troposphere [*Raes*, 1995; *Merikanto et al.*, 2009].

Sulfate aerosols also cause ozone destruction through heterogeneous chemical reactions in the stratosphere [*Peter and Grooß*, 2012] and are important components of present and past atmospheres of other planets of the solar system, such as Venus or Early Mars [*McGouldrick et al.*, 2011].

Besides its tropospheric significance, sulfuric acid -water particle formation mechanism is likely responsible for generating a persistent aerosol layer in the stratosphere (the Junge layer) composed of sulfuric acid-water particles [*Lee et al.*, 2003]. This layer has a predominantly cooling effect on the global climate [*Solomon et al.*, 2011]. Volcanic eruptions inject variable amounts of gaseous sulfur and sulfate particles into the Earth's stratosphere, leading to variations in the sulfate aerosol concentrations [*Vernier et al.*, 2011; *Sawamura et al.*, 2012], while also changes in anthropogenic sulfur dioxide emissions can lead to substantial changes in lower stratospheric sulfate loading [*Pitari et al.*, 2002; *Hofmann et al.*, 2009; *Hommel et al.*, 2015]. These effects need to be taken into account in climate models extending up to the stratosphere.

Venus' clouds, which cover the whole planet, and are responsible for Venus' high visible wavelength albedo [*Esposito et al.*, 1983], are mainly formed of sulfuric acid solution droplets at around 50-70 km above the Venusian surface at conditions comparable to those on the Earth with temperatures and pressures of the order of T=200-350 K and p=0.01-1 bar. These layered clouds distributed over 20 km effectively block the sunlight from reaching the surface of the planet, where only a few percent of solar radiation is received. The surface temperatures on Venus are, however, on average around 700 K because of the greenhouse effect of the very thick CO_2 atmosphere, although without the clouds the planet would be even hotter. It is likely that binary sulfuric acid - water particle formation plays a significant role in the formation of the clouds in Venus. Previous models have assumed [*James et al.*, 1997; *McGouldrick and Toon*, 2007; *Gao et al.*, 2014] that cloud droplet formation involves heterogeneous nucleation of sulfuric acid on pre-existing particles. No observations have allowed the identification of the possible CCN, although several candidates have been suggested [such as sulfur allotropes and meteor dust, *Young*, 1983; *Gao et al.*, 2014]. However, the conditions in Venus could also allow

the droplet formation to be initiated by homogeneous or ion-induced unary/binary nucleation and followed by subsequent growth to cloud droplet sizes.

Large scale atmospheric aerosol models require computationally efficient parameterized representations of dynamics of the particle formation process in various ambient conditions. Such representations can be produced by either calculating theoretical formation rates based on physical properties of the system in different conditions and by parameterizing the data or interpolating from a look-up-table of the data, or by gathering experimental data points and fitting suitable functions to the data. Since particle formation has a complex dependence on the concentrations of participating species and on temperature, the latter approach, while possibly more accurate for describing measured data, is not trustworthy for conditions outside the measurement range. Therefore, it is much safer to base parameterizations on a theory that can reproduce the measured data and predict the dynamics of particle formation outside the measured range.

The physical understanding of atmospheric particle formation processes has not been supported by a firm basis, even for the relatively simple binary sulfuric acid - water system. Different theoretical formulations for binary particle formation for the neutral system [*Wexler et al.*, 1994; *Pandis et al.*, 1994; *Kulmala et al.*, 1998; *Vehkamäki et al.*, 2002; *Kazil and Lovejoy*, 2007; *Yu*, 2008], and for the ion-induced system in particular [*Modgil et al.*, 2005; *Kazil and Lovejoy*, 2007; *Yu*, 2010], can produce binary formation rates that vary by several orders of magnitude [*Zhang et al.*, 2010]. The lack of precision and coverage of binary particle formation experiments that could be used for quantitative validation of theoretical models has also contributed to the variation in the formation rates predicted by the different parameterizations. For example, the theory used by *Yu* [2010] probably contains a double counting of the dipole-dipole interaction [*Donald et al.*, 2008], leading to too high binding energies and predictions of the formation rate [*Donald et al.*, 2011]. New particle formation measurements in controlled conditions [*Duplissy et al.*, 2015] finally allow constraining the theoretical models used.

The Classical Nucleation Theory [CNT, *Doyle*, 1961; *Binder and Stauffer*, 1976; *Trinkaus*, 1983; *Seinfeld and Pandis*, 1998] is an old and elegant description of the nucleation process, but suffers from the assumption of macroscopic bulk properties for the substances at microscopic scales. Recent Cosmics Leaving OUtdoor Droplets (CLOUD) project in CERN has, for the first time, provided accurate and demonstrably contaminant-free measurements of binary sulfuric acid - water particle formation allowing precise model-data comparisons. In the pro-

vided parameterization we use the thermodynamically consistent Classical Nucleation Theory normalized with quantum chemical data on sulfuric acid hydration as described in *Merikanto et al.* [2015]. The model has been validated against the CLOUD experiments [*Duplissy et al.*, 2015]. The framework of Classical Nucleation Theory ensures a physically based behavior for the developed parameterizations even outside the experimental range.

2 Methods

In this paper we present new parameterizations of neutral and ion-induced sulfuric acid-water particle formation. The thermodynamic data and the applied theoretical model used for generating the parameterizations are described in *Merikanto et al.* [2015]. In the framework of the revised theory of *Merikanto et al.* [2015], both neutral and ion-induced particle formation can take place in the range of parameterized conditions either through nucleation, where particle formation involves crossing of the free energy barrier for formation of stable particles, or through kinetic particle formation, where such free energy barrier does not exist. Throughout the paper we generally employ the term ”particle formation” to describe the process in general, but may substitute it with ”nucleation” when the particle formation involves a free energy barrier. When the process is barrierless we use the term kinetic particle formation.

The binary particle formation rates at conditions close to zero relative humidity tend closely towards one-component nucleation rates, but the binary theory cannot mathematically handle zero relative humidity due to singularities in the kinetic prefactor for the nucleation rate in this case. Furthermore, the zero relative humidity limit of the binary kinetic prefactor does not approach exactly the unary prefactor, producing an inconsistency, albeit small, between the binary and unary models. For mathematical completeness, we discuss the difference in binary and unary prefactors in the Appendix. Within the accuracy required for the parameterization, the predicted particle formation approaches one-component sulfuric acid particle formation at very low relative humidities ($x > 0.99$), and at zero relative humidity the one-component theory is used to produce the data. However, the parameterizations do not include the exact RH=0 point, since they contain logarithms of RH.

The neutral sulfuric acid -water parameterization can be viewed as an update to the widely used [*Vehkamäki et al.*, 2002] particle formation parameterization. The temperature and sulfuric acid concentration ranges of the new parameterizations are larger than those of *Vehkamäki et al.* [2002] and *Vehkamäki et al.* [2003], and the calculations are also extended to very low

relative humidities. This was motivated by the present development of sulfuric acid cloud models for the Venusian atmosphere, which is much drier than the Earth's atmosphere.

The model behind the present parameterization differs form the model used in *Vehkamäki et al.* [2002] and *Vehkamäki et al.* [2003] in three respects: first we now use analytical formulae for the second derivatives of the formation free energy, since the numerical derivatives were unstable at the one-component limit. Second, the cluster distribution in the nucleating vapor is normalized via a known reference concentration, which in *Noppel et al.* [2002] and *Vehkamäki et al.* [2002] was taken to be the sulfuric acid dihydrate. Here, here we use the full monomer hydrate distribution in the normalization process instead of only the dihydrate. This modified approach ensures a smooth transition into a one-component system in the pure sulfuric acid limit. Third, the reference sulfuric acid monomer hydrate distribution is based on more accurate quantum chemical results [*Kurtén et al.*, 2007; *Henschel et al.*, 2014] than in *Vehkamäki et al.* [2002] and *Vehkamäki et al.* [2003]

In the presence of water, the total concentration of sulphuric acid molecules can be significantly larger that the concentration of free sulphuric acid monomers, and a large fraction of acid molecules is bound to hydrates. In the conditions of Earth's atmosphere, the concentration of water is approximately ten orders of magnitude higher than that of sulphuric acid, and thus the total concentration of water molecules can be considered equal to the concentration of free water monomers, as pure water cluster formation does not play a significant role either. In the very dry conditions studied in this work, this is not necessarily true and the distinction between total concentration of water and concentration free of water molecules must be kept in mind. By definition relative humidity used as an input parameter in the parameterizations is proportional to the concentration of free water molecules.

3 Size and nature of the ions

If the free energy of formation as a function of cluster size in ion-induced particle formation exhibits a barrier, the equation yielding the critical cluster radius has two solutions: a stable (in one dimensional representation free energy minimum) pre-nucleation cluster representing the ion in surrounded by a few molecules, r_1^*, and the actual metastable (free energy maximum) critical cluster r_2^*. [see Figure 2 of *Merikanto et al.*, 2015]. The classical version of ion-induced nucleation theory used in this work assumes that the size of the bare ion in smaller than the lower radius $r_{\mathrm{ion}} < r_1^*$, and in this case the size of the ion does not affect the en-

ergetics of nucleation. While an extension of the theory to relax this condition is possible, it is beyond the scope of this study. Thus, care should be taken to ensure that the ions are small enough to satisfy this condition always when this parametrization is applied. For the whole validity range of the parametrization the radius r_1^* varies between 0.6 nm - 1.4 nm. Ion size has a very minor effect on the kinetics of nucleation, which has been ignored in this study as this produces an error insignificant compared to other sources of uncertainty in the nucleation rates. We have used ion radius 0.487 nm corresponding to the bisulphate ion in all the calculations.

In the Earths atmosphere, the dominant molecular anions (HSO_4^-, NO_3^-, Cl^-) forming the cores of negatively charged cluster ions are mostly the conjugate bases of the strongest atmospheric acids, which in turn are small inorganic molecules. Similarly, the dominant atmospheric molecular cations tend to be the conjugate acids of the strongest bases (e.g. NH_4^+, pyridium, different aminium ions), though H_3O^+ -based clusters are also often present due to the much larger concentration of water. With the possible exception of some of the nitrogen-containing organic cations, these molecular ions are all rather small - well below 1 nm in diameter [*Hirsikko et al.*, 2011; *Ehn et al.*, 2010; *Beig and Brasseur*, 2000]

Though the precise chemical identities of the acids and bases present of course vary between different planetary atmospheres, the fundamental result that atmospheric molecular ions tend to be rather small is likely universal, especially for the anions. As the complicated large organic molecules present in our atmosphere are almost invariably biogenic, it could even be argued that the probability of encountering large molecular ions should be even smaller in other planetary atmospheres compared to ours.

It should be noted that in cases where the core molecular ions are formed by charging large organic molecules (e.g. biomolecules), application of classical ion-induced nucleation theory may suffer from difficulties above and beyond that related to ion size. In such cases, the negative or positive charge is very likely localized to one or more specific functional group of the molecule (e.g. sulfate, nitrate or carboxylate groups in the case of anions). Thus, treating the molecular ion as a uniformly charged sphere (an excellent approximation for simple inorganic ions such as bisulfate or ammonium) may lead to large errors even if the ion size is appropriately accounted for.

In laboratory conditions, molecular ions of arbitrary size can be created for example in the form of charged metal clusters. In contrast to the charged biomolecules discussed above,

heterogeneous nucleation onto such core ions may in principle be described fairly well by classical theory, as the charge can be delocalized over the entire (more or less spherical) cluster. When applying the classical theory to such studies, the effect of ion size on the nucleation barrier must therefore be taken into account.

4 Particle formation parameterizations

Parameterizations are given for neutral and ion-induced particle formation rates and critical cluster sulfuric acid mole fraction, radius and total number of molecules in the cluster. We also provide parameterizations for the limit at which particle formation becomes kinetic in both neutral and ion-induced cases, that is, the conditions where the free energy barrier limiting the particle formation rate disappears. Analytical equations are given for calculating the particle formation rate in the kinetic regime. Moreover, a parameterization for the threshold sulfuric acid concentration that yield a neutral particle formation rate of 1 $\mathrm{cm^{-3}s^{-1}}$ is given for three separate, but contiguous, temperature ranges (in the lowest temperature range particle formation is kinetic).

In the following we present the parameterizations and compare the obtained theoretical and parameterized results with each other and also, in the neutral case, with the theory and parameterization of *Vehkamäki et al.* [2002].

The validity of the neutral nucleation parameterization is limited to relative humidities from 0.001% to 100%, sulphuric acid concentration from 10^4 to 10^{13} $\mathrm{cm^{-3}}$, and to temperatures from 165 to 400 K. The results of the parameterization are valid only if the resulting particle formation rate is $J > 10^{-7}\mathrm{cm^{-3}s^{-1}}$ and the number of sulfuric acid molecules in the critical cluster is $n_a^* > 1$. The limit $n_a^* = 1$ is related to particle formation becoming kinetic. We have developed another parameterization that gives the sulfuric acid concentration required for the kinetic limit as a function of relative humidity and temperature.

The validity of the ion-induced nucleation parameterization is limited to relative humidities from 10^{-5} % to 100%, sulphuric acid concentration from 10^4 to 10^{16} $\mathrm{cm^{-3}}$, and the temperature range 195-400 K. The results of the parameterization are valid only if the resulting particle formation rate (assuming a negative ion concentration of 1 $\mathrm{cm^{-3}}$) is $J > 10^{-10}\mathrm{cm^{-3}s^{-1}}$ and, as for the neutral case, total number of sulfuric acid molecules in the critical cluster is $n_a^* > 1$, since below this limit particle formation becomes again kinetic. This ion-induced kinetic limit is described by another parameterization. The ion-induced particle formation rate

has to be multiplied by the actual negative ion concentration (typically some hundreds to some thousand negative ions cm^{-3}) to get rates in the conditions investigated. Depending on the chemistry of the atmosphere studied, negative ion concentration can depend on the sulphuric acid concentration and vice versa. As the input values of our parameterization, these two concentrations are treated as independent variables, and the coupling between them in the studied case can be specified before calling the parametrization.

The particle formation calculations using the parameterizations are orders of magnitude more computationally efficient than with the full theory, and hence the parameterizations are suitable for large scale atmospheric models. A Fortran code for the new parameterization is included in the supplementary electronic material. When using the parameterizations in, for example, a microphysical/atmospheric model, it is advisable to use the same thermodynamical data (density, surface tension, activities, etc., see *Merikanto et al.* [2015]) as used here for consistency, and double precision for floats should be used.

4.1 Neutral particle formation

The mole fraction of sulfuric acid in the critical cluster, valid for both neutral and ion-induced case, is given by

$$\begin{aligned} x^* \quad = \quad & 7.9036365428891719 \cdot 10^{-1} - 2.8414059650092153 \cdot 10^{-3}\, T \\ & +1.4976802556584141 \cdot 10^{-2}\, \ln(\rho_a) - 2.4511581740839115 \cdot 10^{-4}\, T\, \ln(\rho_a) \\ & +3.4319869471066424 \cdot 10^{-3}\, \ln(\frac{RH}{100}) - 2.8799393617748428 \cdot 10^{-5}\, T\, \ln(\frac{RH}{100}) \\ & +3.0174314126331765 \cdot 10^{-4} \left[\ln(\frac{RH}{100})\right]^2 - 2.2673492408841294 \cdot 10^{-6}\, T \left[\ln(\frac{RH}{100})\right]^2 \\ & -4.3948464567032377 \cdot 10^{-3} \left[\ln(\frac{RH}{100})\right]^3 + 5.3305314722492146 \cdot 10^{-5}\, T \left[\ln(\frac{RH}{100})\right]^3, \end{aligned} \tag{1}$$

where ρ_a is the total gas phase concentration of sulfuric acid (1/cm^3), T is the absolute temperature and RH is the relative humidity in %.

The particle formation rate is given by an exponential of a third order polynomial of $\ln(RH/100)$ and $\ln(\rho_a)$

$$
\begin{aligned}
J[1/(\mathrm{cm}^3\mathrm{s})] = \exp\{ & a(T,x^*) \\
& + b(T,x^*)\ln(RH/100) + c(T,x^*)[\ln(RH/100)]^2 \\
& + d(T,x^*)[\ln(RH/100)]^3 + e(T,x^*)\ln(\rho_a) \\
& + f(T,x^*)\ln(RH/100)\ln(\rho_a) \\
& + g(T,x^*)[\ln(RH/100)]^2\ln(\rho_a) \\
& + h(T,x^*)[\ln(\rho_a)]^2 \\
& + i(T,x^*)\ln(RH/100)[\ln(\rho_a)]^2 \\
& + j(T,x^*)[\ln(\rho_a)]^3 \}\,,
\end{aligned}
\tag{2}
$$

where the coefficients $a(T,x^*)\ldots j(T,x^*)$ are functions of temperature and critical cluster mole fraction x^* (calculated using equation (1)):

$$
\begin{aligned}
a(T,x^*) &= 2.1361182605986115\cdot 10^{-1} + 3.3827029855551838\,T - 3.2423555796175563\cdot 10^{-2}\,T^2 \\
&\quad +7.0120069477221989\cdot 10^{-5}\,T^3 + \frac{8.0286874752695141}{x^*} \\
b(T,x^*) &= -2.6939840579762231\cdot 10^{-1} + 1.6079879299099518\,T - 1.9667486968141933\cdot 10^{-2}\,T^2 \\
&\quad +5.5244755979770844\cdot 10^{-5}\,T^3 + \frac{7.8884704837892468}{x^*} \\
c(T,x^*) &= 4.6374659198909596 - 8.2002809894792153\cdot 10^{-2}\,T + 8.5077424451172196\cdot 10^{-4}\,T^2 \\
&\quad -2.6518510168987462\cdot 10^{-6}\,T^3 - \frac{1.4625482500575278}{x^*} \\
d(T,x^*) &= -5.2413002989192037\cdot 10^{-1} + 5.2755117653715865\cdot 10^{-3}\,T - 2.9491061332113830\cdot 10^{-6}\,T^2 \\
&\quad -2.4815454194486752\cdot 10^{-8}\,T^3 - \frac{5.2663760117394626\cdot 10^{-2}}{x^*} \\
e(T,x^*) &= 1.6496664658266762 - 8.0809397859218401\cdot 10^{-1}\,T + 8.9302927091946642\cdot 10^{-3}\,T^2 \\
&\quad -1.9583649496497497\cdot 10^{-5}\,T^3 - \frac{8.9505572676891685}{x^*} \\
f(T,x^*) &= -3.0025283601622881\cdot 10^{1} + 3.0783365644763633\cdot 10^{-1}\,T - 7.4521756337984706\cdot 10^{-4}\,T^2 \\
&\quad -5.7651433870681853\cdot 10^{-7}\,T^3 + \frac{1.2872868529673207}{x^*} \\
g(T,x^*) &= -6.1739867501526535\cdot 10^{-1} + 7.2347385705333975\cdot 10^{-3}\,T - 3.0640494530822439\cdot 10^{-5}\,T^2 \\
&\quad 6.5944609194346214\cdot 10^{-8}\,T^3 - \frac{2.8681650332461055\cdot 10^{-2}}{x^*} \\
h(T,x^*) &= 6.5213802375160306 - 4.7907162004793016\cdot 10^{-2}\,T - 1.0727890114215117\cdot 10^{-4}\,T^2 \\
&\quad +5.6401818280534507\cdot 10^{-7}\,T^3 + \frac{5.4113070888923009\cdot 10^{-1}}{x^*} \\
i(T,x^*) &= 5.2062808476476330\cdot 10^{-1} - 6.0696882500824584\cdot 10^{-3}\,T + 2.3851383302608477\cdot 10^{-5}\,T^2 \\
&\quad -1.5243837103067096\cdot 10^{-8}\,T^3 - \frac{5.6543192378015687\cdot 10^{-2}}{x^*} \\
j(T,x^*) &= -1.1630806410696815\cdot 10^{-1} + 1.3806404273119610\cdot 10^{-3}\,T - 2.0199865087650833\cdot 10^{-6}\,T^2 \\
&\quad -3.0200284885763192\cdot 10^{-9}\,T^3 - \frac{6.9425267104126316\cdot 10^{-3}}{x^*}.
\end{aligned}
$$

The total number of molecules in the critical cluster $n^*_{\mathrm{tot}} = n^*_a + n^*_w$ (where n^*_w is the number of water molecules in the critical cluster) is given by

$$
\begin{aligned}
n^*_{\mathrm{tot}} = \exp\{ & A(T,x^*) \\
& + B(T,x^*)\ln(RH/100) + C(T,x^*)[\ln(RH/100)]^2 \\
& + D(T,x^*)[\ln(RH/100)]^3 + E(T,x^*)\ln(\rho_a) \\
& + F(T,x^*)\ln(RH/100)\ln(\rho_a) \\
& + G(T,x^*)[\ln(RH/100)]^2\ln(\rho_a) \\
& + H(T,x^*)[\ln(\rho_a)]^2 \\
& + I(T,x^*)\ln(RH/100)[\ln(\rho_a)]^2 \\
& + J(T,x^*)[\ln(\rho_a)]^3\},
\end{aligned}
\tag{3}
$$

where the coefficients $A(T,x^*) \ldots J(T,x^*)$ again depend on temperature and critical cluster mole fraction x^* (from equation (1)):

$$
\begin{aligned}
A(T,x^*) &= -3.5863435141979573\cdot 10^{-3} - 1.0098670235841110\cdot 10^{-1}\,T + 8.9741268319259721\cdot 10^{-4}\,T^2 \\
&\quad -1.4855098605195757\cdot 10^{-6}\,T^3 - \frac{1.2080330016937095\cdot 10^{-1}}{x^*} \\
B(T,x^*) &= 1.1902674923928015\cdot 10^{-3} - 1.9211358507172177\cdot 10^{-2}\,T + 2.4648094311204255\cdot 10^{-4}\,T^2 \\
&\quad -7.5641448594711666\cdot 10^{-7}\,T^3 - \frac{2.0668639384228818\cdot 10^{-2}}{x^*} \\
C(T,x^*) &= -3.7593072011595188\cdot 10^{-2} + 9.0993182774415718\cdot 10^{-4}\,T - 9.5698412164297149\cdot 10^{-6}\,T^2 \\
&\quad +3.7163166416110421\cdot 10^{-8}\,T^3 + \frac{1.1026579525210847\cdot 10^{-2}}{x^*} \\
D(T,x^*) &= 1.1530844115561925\cdot 10^{-2} - 1.8083253906466668\cdot 10^{-4}\,T + 8.0213604053330654\cdot 10^{-7}\,T^2 \\
&\quad -8.5797885383051337\cdot 10^{-10}\,T^3 + \frac{1.0243693899717402\cdot 10^{-3}}{x^*} \\
E(T,x^*) &= -1.7248695296299649\cdot 10^{-2} + 1.1294004162437157\cdot 10^{-2}\,T - 1.2283640163189278\cdot 10^{-4}\,T^2 \\
&\quad +2.7391732258259009\cdot 10^{-7}\,T^3 + \frac{6.8505583974029602\cdot 10^{-2}}{x^*} \\
F(T,x^*) &= 2.9750968179523635\cdot 10^{-1} - 3.6681154503992296\cdot 10^{-3}\,T + 1.0636473034653114\cdot 10^{-5}\,T^2 \\
&\quad +5.8687098466515866\cdot 10^{-9}\,T^3 - \frac{5.2028866094191509\cdot 10^{-3}}{x^*} \\
G(T,x^*) &= 7.6971988880587231\cdot 10^{-4} - 2.4605575820433763\cdot 10^{-5}\,T + 2.3818484400893008\cdot 10^{-7}\,T^2 \\
&\quad -8.8474102392445200\cdot 10^{-10}\,T^3 - \frac{1.6640566678168968\cdot 10^{-4}}{x^*} \\
H(T,x^*) &= -7.7390093776705471\cdot 10^{-2} + 5.8220163188828482\cdot 10^{-4}\,T + 1.2291679321523287\cdot 10^{-6}\,T^2 \\
&\quad -7.4690997508075749\cdot 10^{-9}\,T^3 - \frac{5.6357941220497648\cdot 10^{-3}}{x^*} \\
I(T,x^*) &= -4.7170109625089768\cdot 10^{-3} + 6.9828868534370193\cdot 10^{-5}\,T - 3.1738912157036403\cdot 10^{-7}\,T^2 \\
&\quad +2.3975538706787416\cdot 10^{-10}\,T^3 + \frac{4.2304213386288567\cdot 10^{-4}}{x^*} \\
J(T,x^*) &= 1.3696520973423231\cdot 10^{-3} - 1.6863387574788199\cdot 10^{-5}\,T + 2.7959499278844516\cdot 10^{-8}\,T^2 \\
&\quad +3.9423927013227455\cdot 10^{-11}\,T^3 + \frac{8.6136359966337272\cdot 10^{-5}}{x^*}.
\end{aligned}
$$

The radius of the critical cluster is given as a function of the mole fraction and the total number of molecules in the cluster:

$$r^*[\mathrm{nm}] = \exp[-22.378268374023630 + 0.44462953606125100\,x^* + 0.33499495707849131\ln(n^*_{\mathrm{tot}})]. \tag{4}$$

We also present a parameterization for the threshold total concentration of sulfuric acid that gives particle formation rate J=1 cm^{-3}s^{-1}. The threshold concentration depends on the temperature and the relative humidity as given in the following equations. We divided the temperature range in three parts (155-185 K, where particle formation is in the kinetic range, 190-310 K and 310-400 K) to ensure a good quality of the fits. The smallest RH used for fitting is 5% ($S = 5{\cdot}10^{-2}$). We have included sulfuric acid concentrations above 10^{13} cm^{-3} (which were excluded from the parameterizations of J, x, $n_{\rm tot}$ and r^*) to enable the threshold parameterization to extend to the whole RH range also at high temperatures. For the (nucleation) range 310-400 K the threshold concentration parameterization is

$$\begin{aligned}\rho_a^{J=1}[1/\mathrm{cm}^3] = \exp\Bigg[&-2.8220714121794250 + 1.1492362322651116\cdot 10^{1}\,\frac{RH}{100} \\ &-\frac{3.3034839106184218\cdot 10^{3}}{T} - \frac{7.1828571490168133\cdot 10^{2}}{T}\frac{RH}{100} + 1.4649510835204091\cdot 10^{-1}\,T \\ &-3.0442736551916524\cdot 10^{-2}\,\frac{RH}{100}\,T - 9.3258567137451497\cdot 10^{-5}\,T^2 \\ &-1.1583992506895649\cdot 10^{1}\,\ln(\frac{RH}{100}) + \frac{1.5184848765906165\cdot 10^{3}\,\ln(\frac{RH}{100})}{T} \\ &+1.8144983916747057\cdot 10^{-2}\,T\,\ln(\frac{RH}{100})\Bigg],\end{aligned} \tag{5}$$

and for the (nucleation) range 190-310 K:

$$\begin{aligned}\rho_a^{J=1}[1/\mathrm{cm}^3] = \exp\Bigg[&-3.1820396091231999\cdot 10^{2} + 7.2451289153199676\,\frac{RH}{100} \\ &+\frac{2.6729355170089486\cdot 10^{4}}{T} - \frac{7.1492506076423069\cdot 10^{2}}{T}\frac{RH}{100} + 1.2617291148391978\,T \\ &-1.6438112080468487\cdot 10^{-2}\,\frac{RH}{100}\,T - 1.4185518234553220\cdot 10^{-3}\,T^2 \\ &-9.2864597847386694\,\ln(\frac{RH}{100}) + \frac{1.2607421852455602\cdot 10^{3}\,\ln(\frac{RH}{100})}{T} \\ &+1.3324434472218746\cdot 10^{-2}\,T\,\ln(\frac{RH}{100})\Bigg].\end{aligned} \tag{6}$$

For the range 155-185 K where particle formation is kinetic, the threshold concentration parameterization is:

$$\begin{aligned}\rho_a^{J=1}[1/\mathrm{cm}^3] &= 1.1788859232398459\cdot 10^{5} - 1.0244255702550814\cdot 10^{4}\cdot\frac{RH}{100} \\ &+ 4.6815029684321962\cdot 10^{3}\cdot(\frac{RH}{100})^2 - 1.6755952338499657\cdot 10^{2}\cdot T.\end{aligned} \tag{7}$$

The following equations give the parameterization for the total concentration of sulfuric acid at the kinetic limit (as a function of RH and T). These equations are to be used to check if the conditions are such that particle formation is kinetic, in which case the Eqs. (11) and (12) should be used to calculate the particle formation rate instead of Eq. (2). Here we

divided the relative humidity range in three parts (RH=1%–100%, 0.01% – 1% and 0.0005% – 0.01%) to ensure a good quality of the fits. The kinetic limit sulfuric acid concentration (above which particle formation is kinetic) for RH=1%–100% is:

$$\begin{aligned}\rho_a^{\mathrm{kin}}[1/\mathrm{cm}^3] = \exp\Bigg[&7.8920778706888086\cdot 10^1 + 7.3665492897447082\,\frac{RH}{100} \\ &-\frac{1.2420166571163805\cdot 10^4}{T} - \frac{6.1831234251470971\cdot 10^2}{T}\,\frac{RH}{100} - 2.4501159970109945\cdot 10^{-2}\,T \\ &-1.3463066443605762\cdot 10^{-2}\,\frac{RH}{100}\,T + 8.3736373989909194\cdot 10^{-6}\,T^2 \\ &-1.4673887785408892\,\ln(\frac{RH}{100}) - \frac{3.2141890006517094\cdot 10^1\ \ln(\frac{RH}{100})}{T} \\ &+2.7137429081917556\cdot 10^{-3}\,T\ \ln(\frac{RH}{100})\Bigg]\,.\end{aligned} \tag{8}$$

The kinetic limit sulfuric acid concentration for RH=0.01%–1% is:

$$\begin{aligned}\rho_a^{\mathrm{kin}}[1/\mathrm{cm}^3] = \exp\Bigg[&7.9074383049843647\cdot 10^1 - 2.8746005462158347\cdot 10^1\,\frac{RH}{100} \\ &-\frac{1.2070272068458380\cdot 10^4}{T} - \frac{5.9205040320056632\cdot 10^3}{T}\,\frac{RH}{100} - 2.4800372593452726\cdot 10^{-2}\,T \\ &-4.3983007681295948\cdot 10^{-2}\,\frac{RH}{100}\,T + 2.5943854791342071\cdot 10^{-5}\,T^2 \\ &-2.3141363245211317\,\ln(\frac{RH}{100}) + \frac{9.9186787997857735\cdot 10^1\ \ln(\frac{RH}{100})}{T} \\ &+5.6819382556144681\cdot 10^{-3}\,T\ \ln(\frac{RH}{100})\Bigg]\,.\end{aligned} \tag{9}$$

The kinetic limit sulfuric acid concentration for RH=0.0005%–0.01% is:

$$\begin{aligned}\rho_a^{\mathrm{kin}}[1/\mathrm{cm}^3] = \exp\Bigg[&8.5599712000361677\cdot 10^1 + 2.7335119660796581\cdot 10^3\,\frac{RH}{100} \\ &-\frac{1.1842350246291651\cdot 10^4}{T} - \frac{1.2439843468881438\cdot 10^6}{T}\,\frac{RH}{100} - 5.4536964974944230\cdot 10^{-2}\,T \\ &+5.0886987425326087\,\frac{RH}{100}\,T + 7.1964722655507067\cdot 10^{-5}\,T^2 \\ &-2.4472627526306372\,\ln(\frac{RH}{100}) + \frac{1.7561478001423779\cdot 10^2\ \ln(\frac{RH}{100})}{T} \\ &+6.2640132818141811\cdot 10^{-3}\,T\ \ln(\frac{RH}{100})\Bigg]\,.\end{aligned} \tag{10}$$

The neutral particle formation rate in the kinetic range (J_{kin}) can be easily calculated via the following equations [*Merikanto et al.*, 2015]:

$$J_{\mathrm{kin,neutral}} = \frac{C}{2}\sqrt{T}(\rho_a^{\mathrm{total}})^2 \tag{11}$$

where

$$C = (r_a + r_{\mathrm{ref}})^2\sqrt{8\pi k\left(\frac{1}{m_a} + \frac{1}{m_{\mathrm{ref}}}\right)} \tag{12}$$

where $r_{\mathrm{ref}} = r_a = 0.3\cdot 10^{-9}$m and $m_{\mathrm{ref}} = m_a = 1.661\cdot 10^{-27}$kg in the neutral particle formation case.

4.2 Ion-induced particle formation

In the following we present the parameterizations for ion-induced particle formation rate, the number of molecules in the critical cluster and the critical cluster radius as functions of ρ_a, the total gas phase concentration of sulfuric acid (cm^{-3}), T, the absolute temperature, and RH, the relative humidity in %. The kinetic limit sulfuric acid concentration parameterization is given as a function of temperature T and relative humidity RH. Note that the critical cluster mole fraction can be solved from the same equation for both neutral and ion-induced particle formation [see Eq. (6) of *Merikanto et al.*, 2015, and the references therein], and thus the same mole fraction parameterization (Eq. (1)) can be used for both particle formation types.

The ion-induced particle formation rate for the assumed negative ion concentration of 1 cm^{-3} is given by the following dependence on $\ln(RH/100)$ and $\ln(\rho_a)$ (the actual particle formation rate is obtained by multiplying with the actual ion concentration in cm^{-3}):

$$
\begin{aligned}
J \;=\; & \exp\left[f_1^J(T) + f_2^J(T)\cdot\left[\ln(\frac{RH}{100})\right]^{-2} + f_3^J(T)\cdot\left[\ln(\frac{RH}{100})\right]^{-2}\cdot\ln\rho_a \right. \\
& + f_4^J(T)\cdot\left[\ln(\frac{RH}{100})\right]^{-1}\cdot\ln^{-1}\rho_a + f_5^J(T)\cdot\left[\ln(\frac{RH}{100})\right]^{-1} + f_6^J(T)\cdot\left[\ln(\frac{RH}{100})\right]^{-1}\cdot\ln\rho_a \\
& + f_7^J(T)\cdot\left[\ln(\frac{RH}{100})\right]^{-1}\cdot\ln^2\rho_a + f_8^J(T)\cdot\left[\ln(\frac{RH}{100})\right]^{-1}\cdot\ln^3\rho_a + f_9^J(T)\cdot\ln^{-2}\rho_a + f_{10}^J(T)\cdot\ln^{-1}\rho_a \\
& + f_{11}^J(T)\cdot\ln\rho_a + f_{12}^J(T)\cdot\ln^2\rho_a + f_{13}^J(T)\cdot\ln^3\rho_a + f_{14}^J(T)\cdot\ln(\frac{RH}{100})\cdot\ln^{-2}\rho_a \\
& + f_{15}^J(T)\cdot\ln(\frac{RH}{100})\cdot\ln^{-1}\rho_a + f_{16}^J(T)\cdot\ln(\frac{RH}{100}) + f_{17}^J(T)\cdot\ln(\frac{RH}{100})\cdot\ln\rho_a + f_{18}^J(T)\cdot\ln(\frac{RH}{100})\cdot\ln^2\rho_a \\
& + f_{19}^J(T)\cdot\ln(\frac{RH}{100})\cdot\ln^3\rho_a + f_{20}^J(T)\cdot\left[\ln(\frac{RH}{100})\right]^2\cdot\ln^{-1}\rho_a + f_{21}^J(T)\cdot\left[\ln(\frac{RH}{100})\right]^2 \\
& \left. + f_{22}^J(T)\cdot\left[\ln(\frac{RH}{100})\right]^2\cdot\ln\rho_a + f_{23}^J(T)\cdot\left[\ln(\frac{RH}{100})\right]^2\cdot\ln^2\rho_a + f_{24}^J(T)\cdot\frac{RH}{100}\right],
\end{aligned}
\tag{13}
$$

where the coefficients f_N^J are functions of temperature T as follows:

$$
f_N^J(T) = a_{1,N} + a_{2,N}\cdot T + a_{3,N}\cdot T^2 + a_{4,N}\cdot T^3 + a_{5,N}\cdot T^{-1}, \tag{14}
$$

and the coefficients $a_{1-5,N}$ for each $f_N^J(T)$ are given in Table 1.

Table 1. Coefficients $a_{1-5,N}$ of Eq. (14).

N	$a_{1,N}$	$a_{2,N}$	$a_{3,N}$	$a_{4,N}$	$a_{5,N}$
1	$3.0108954259038608 \cdot 10^{1}$	$6.1176722090512577 \cdot 10^{1}$	$8.7240333618891663 \cdot 10^{-1}$	$-4.6191788649375719 \cdot 10^{-3}$	$8.3537059107024481 \cdot 10^{-1}$
2	$1.5028549216690628 \cdot 10^{1}$	$-1.9310989753720623 \cdot 10^{-1}$	$8.0155514634860480 \cdot 10^{-4}$	$-1.0832730707799128 \cdot 10^{-6}$	1.7577660457989019
3	$-2.0487870170216488 \cdot 10^{-1}$	$1.3263949252910405 \cdot 10^{-3}$	$-8.4195688402450274 \cdot 10^{-6}$	$1.6154895940993287 \cdot 10^{-8}$	$3.8734212545203874 \cdot 10^{1}$
4	1.4955918863858371	$9.2290004245522454 \cdot 10^{1}$	$-8.9006965195392618 \cdot 10^{-1}$	$2.2319123411013099 \cdot 10^{-3}$	$4.0180079996840852 \cdot 10^{-3}$
5	7.9018031228561085	$-1.1649433968658949 \cdot 10^{1}$	$1.1400827854910951 \cdot 10^{-1}$	$-3.1941526492127755 \cdot 10^{-4}$	$-3.7662115740271446 \cdot 10^{-1}$
6	$1.5725237111225979 \cdot 10^{2}$	-1.0051649979836277	$1.1866484014507624 \cdot 10^{-3}$	$7.3557614998540389 \cdot 10^{-6}$	2.6270197023115189
7	$-1.6973840122470968 \cdot 10^{1}$	$1.1258423691432135 \cdot 10^{-1}$	$-2.9850139351463793 \cdot 10^{-4}$	$1.4301286324827064 \cdot 10^{-7}$	$1.3163389235253725 \cdot 10^{1}$
8	-1.0399591631839757	$2.7022055588257691 \cdot 10^{-3}$	$-2.1507467231330936 \cdot 10^{-6}$	$3.8059489037584171 \cdot 10^{-10}$	$1.5000492788553410 \cdot 10^{2}$
9	1.2250990965305315	$3.0495946490079444 \cdot 10^{1}$	$2.1051563135187106 \cdot 10^{1}$	$-8.2200682916580878 \cdot 10^{-2}$	$2.9965871386685029 \cdot 10^{-2}$
10	4.8281605955680433	$1.7346551710836445 \cdot 10^{2}$	$-1.0113602140796010 \cdot 10^{1}$	$3.7482518458685089 \cdot 10^{-2}$	$-1.4449998158558205 \cdot 10^{-1}$
11	$2.3399230964451237 \cdot 10^{2}$	$-2.3099267235261948 \cdot 10^{1}$	$8.0122962140916354 \cdot 10^{-2}$	$6.1542576994557088 \cdot 10^{-5}$	5.3718413254843007
12	$1.0299715519499360 \cdot 10^{2}$	$-6.4663357203364136 \cdot 10^{-2}$	$-2.0487150565050316 \cdot 10^{-3}$	$8.7935289055530897 \cdot 10^{-7}$	$3.6013204601215229 \cdot 10^{1}$
13	-3.5452115439584042	$1.7083445731159330 \cdot 10^{-2}$	$-1.2552625290862626 \cdot 10^{-5}$	$1.2968447449182847 \cdot 10^{-9}$	$1.5748687512056560 \cdot 10^{2}$
14	2.2338490119517975	$1.0229410216045540 \cdot 10^{2}$	-3.2103611955174052	$1.3397152304977591 \cdot 10^{-2}$	$-2.4155187776460030 \cdot 10^{-2}$
15	3.7592282990713963	$-1.5257988769009816 \cdot 10^{2}$	2.6113805420558802	$-9.0380721653694363 \cdot 10^{-3}$	$-1.3974197138171082 \cdot 10^{-1}$
16	$1.8293600730573988 \cdot 10^{1}$	$1.8344728606002992 \cdot 10^{1}$	$-4.0063363221106751 \cdot 10^{-1}$	$1.4842749371258522 \cdot 10^{-3}$	1.1848846003282287
17	$-1.7634531623032314 \cdot 10^{2}$	4.9011762441271278	$-1.3195821562746339 \cdot 10^{-2}$	$-2.8668619526430859 \cdot 10^{-5}$	$-2.9823396976393551 \cdot 10^{-1}$
18	$-3.2944043694275727 \cdot 10^{1}$	$1.2517571921051887 \cdot 10^{-1}$	$8.3239769771186714 \cdot 10^{-5}$	$2.8191859341519507 \cdot 10^{-7}$	$-2.7352880736682319 \cdot 10^{1}$
19	-1.1451811137553243	$2.0625997485732494 \cdot 10^{-3}$	$-3.4225389469233624 \cdot 10^{-6}$	$4.4437613496984567 \cdot 10^{-10}$	$1.8666644332606754 \cdot 10^{2}$
20	$3.2270897099493567 \cdot 10^{1}$	$7.7898447327513687 \cdot 10^{-1}$	$-6.5662738484679626 \cdot 10^{-3}$	$3.7899330796456790 \cdot 10^{-6}$	$7.1106427501756542 \cdot 10^{-1}$
21	$-2.8901906781697811 \cdot 10^{1}$	-1.5356398793054860	$1.9267271774384788 \cdot 10^{-2}$	$-5.3886270475516162 \cdot 10^{-5}$	$5.0490415975693426 \cdot 10^{-1}$
22	$3.3365683645733924 \cdot 10^{1}$	$-3.6114561564894537 \cdot 10^{-1}$	$9.2977354471929262 \cdot 10^{-4}$	$1.9549769069511355 \cdot 10^{-7}$	-8.8865930095112855
23	2.4592563042806375	$-8.3227071743101084 \cdot 10^{-3}$	$8.2563338043447783 \cdot 10^{-6}$	$-8.4374976698593496 \cdot 10^{-9}$	$-2.0938173949893473 \cdot 10^{2}$
24	$4.4099823444352317 \cdot 10^{1}$	2.5915665826835252	$-1.6449091819482634 \cdot 10^{-2}$	$2.6797249816144721 \cdot 10^{-5}$	$5.5045672663909995 \cdot 10^{-1}$

The number of molecules in the critical cluster in the ion-induced case can be calculated as a function of $\ln(RH/100)$ and $\ln(\rho_a)$ with the following expression:

$$
\begin{aligned}
n^*_{\mathrm{tot}} \quad = \quad & \left| \left(f^n_1(T) + f^n_2(T) \cdot \left[\ln(\frac{RH}{100}) \right]^{-2} \cdot \ln^{-2} \rho_a + f^n_3(T) \cdot \left[\ln(\frac{RH}{100}) \right]^{-2} \right. \right. \\
& + f^n_4(T) \cdot \left[\ln(\frac{RH}{100}) \right]^{-2} \cdot \ln \rho_a + f^n_5(T) \cdot \left[\ln(\frac{RH}{100}) \right]^{-1} \cdot \ln^{-2} \rho_a + f^n_6(T) \cdot \left[\ln(\frac{RH}{100}) \right]^{-1} \cdot \ln^{-1} \rho_a \\
& + f^n_7(T) \cdot \left[\ln(\frac{RH}{100}) \right]^{-1} + f^n_8(T) \cdot \left[\ln(\frac{RH}{100}) \right]^{-1} \cdot \ln \rho_a + f^n_9(T) \cdot \ln^{-2} \rho_a + f^n_{10}(T) \cdot \ln^{-1} \rho_a \\
& + f^n_{11}(T) \cdot \ln \rho_a + f^n_{12}(T) \cdot \ln^2 \rho_a + f^n_{13}(T) \cdot \ln(\frac{RH}{100}) \cdot \ln^{-2} \rho_a + f^n_{14}(T) \cdot \ln(\frac{RH}{100}) \cdot \ln^{-1} \rho_a \\
& + f^n_{15}(T) \cdot \ln(\frac{RH}{100}) + f^n_{16}(T) \cdot \ln(\frac{RH}{100}) \cdot \ln \rho_a + f^n_{17}(T) \cdot \left[\ln(\frac{RH}{100}) \right]^2 + f^n_{18}(T) \cdot \left[\ln(\frac{RH}{100}) \right]^2 \cdot \ln^{-1} \rho_a \\
& \left. \left. + f^n_{19}(T) \cdot \left[\ln(\frac{RH}{100}) \right]^{-3} + f^n_{20}(T) \cdot \frac{RH}{100} \cdot \ln \rho_a + f^n_{21}(T) \cdot \frac{RH}{100} + f^n_{22}(T) \cdot \frac{RH}{100} \cdot \ln^2 \rho_a \right) \right|
\end{aligned}
\tag{15}
$$

where the coefficients f^n_N are functions of temperature T as follows:

$$
f^n_N(T) = b_{1,N} + b_{2,N} \cdot T + b_{3,N} \cdot T^2 + b_{4,N} \cdot T^{-1} + b_{5,N} \cdot T^3 \tag{16}
$$

and the coefficients $b_{1-5,N}$ for each $f^n_N(T)$ are given in Table 2.

The critical cluster radius for ion-induced particle formation can be evaluated using the following expression:

$$
\begin{aligned}
r^* \quad = \quad & f^r_1(T) + f^r_2(T) \cdot \left[\ln(\frac{RH}{100}) \right]^{-2} \cdot \ln^{-1} \rho_a + f^r_3(T) \cdot \left[\ln(\frac{RH}{100}) \right]^{-2} \\
& + f^r_4(T) \cdot \left[\ln(\frac{RH}{100}) \right]^{-2} \cdot \ln \rho_a + f^r_5(T) \cdot \left[\ln(\frac{RH}{100}) \right]^{-1} \cdot \ln^{-2} \rho_a + f^r_6(T) \cdot \left[\ln(\frac{RH}{100}) \right]^{-1} \cdot \ln^{-1} \rho_a \\
& + f^r_7(T) \cdot \left[\ln(\frac{RH}{100}) \right]^{-1} + f^r_8(T) \cdot \left[\ln(\frac{RH}{100}) \right]^{-1} \cdot \ln \rho_a + f^r_9(T) \cdot \left[\ln(\frac{RH}{100}) \right]^{-1} \cdot \ln^2 \rho_a \\
& + f^r_{10}(T) \cdot \ln^{-2} \rho_a + f^r_{11}(T) \cdot \ln^{-1} \rho_a + f^r_{12}(T) \cdot \ln \rho_a + f^r_{13}(T) \cdot \ln^2 \rho_a \\
& + f^r_{14}(T) \cdot \ln(\frac{RH}{100}) \cdot \ln^{-2} \rho_a + f^r_{15}(T) \cdot \ln(\frac{RH}{100}) \cdot \ln^{-1} \rho_a + f^r_{16}(T) \cdot \ln(\frac{RH}{100}) \\
& + f^r_{17}(T) \cdot \ln(\frac{RH}{100}) \cdot \ln \rho_a + f^r_{18}(T) \cdot \ln(\frac{RH}{100}) \cdot \ln^2 \rho_a + f^r_{19}(T) \cdot \left[\ln(\frac{RH}{100}) \right]^2 \cdot \ln^{-1} \rho_a \\
& + f^r_{20}(T) \cdot \left[\ln(\frac{RH}{100}) \right]^2 + f^r_{21}(T) \cdot \left[\ln(\frac{RH}{100}) \right]^2 \cdot \ln \rho_a + f^r_{22}(T) \cdot \left[\ln(\frac{RH}{100}) \right]^3 \cdot \ln \rho_a
\end{aligned}
\tag{17}
$$

where the coefficients f^r_N are functions of temperature T as follows:

$$
f^r_N(T) = c_{1,N} + c_{2,N} \cdot T + c_{3,N} \cdot T^2 + c_{4,N} \cdot T^3 \tag{18}
$$

and the coefficients $c_{1-4,N}$ for each $f^r_N(T)$ are given in Table 3.

Table 2. Coefficients $b_{1-5,N}$ of the Eq. (15).

N	$b_{1,N}$	$b_{2,N}$	$b_{3,N}$	$b_{4,N}$	$b_{5,N}$
1	-4.8324296064013375·10^{4}	5.0469120697428906·10^{2}	-1.1528940488496042	-8.6892744676239192·10^{2}	4.0030302028120469·10^{-4}
2	-6.7259105232039847·10^{3}	1.9197488157452008·10^{2}	-1.3602976930126354	-1.1212637938360332·10^{2}	2.8515597265933207·10^{-3}
3	2.6216455217763342·10^{2}	-2.3687553252750821	7.4074554767517521·10^{-3}	-1.9213956820114927·10^{3}	-9.3839114856129453·10^{-6}
4	3.9652478944137344	1.2469375098256536·10^{-2}	-9.9837754694045633·10^{-5}	-5.1919499210175138·10^{2}	1.6489001324583862·10^{-7}
5	2.4975714429096206·10^{2}	1.7107594562445172·10^{2}	-7.8988711365135289·10^{-1}	-2.2243599782483177·10^{1}	-1.6291523004095427·10^{-4}
6	-8.9270715592533611·10^{2}	1.2053538883338946·10^{2}	-1.5490408828541018	-1.1243275579419826·10^{1}	4.8053105606904655·10^{-3}
7	7.6426441642091631·10^{3}	-7.1785462414656578·10^{1}	2.3851864923199523·10^{-1}	8.5591775688708395·10^{1}	-3.7000473243342858·10^{-4}
8	-5.1516826398607911·10^{1}	9.1385720811460558·10^{-1}	-3.5477100262158974·10^{-3}	2.7545544507625586·10^{3}	5.4708262093640928·10^{-6}
9	-3.0386767129196176·10^{2}	-1.1033438883583569·10^{4}	8.1296859732896067·10^{1}	1.2625883141097162·10^{1}	-1.2728497822219101·10^{-1}
10	-3.3763494256461472·10^{3}	3.1916579136391006·10^{3}	-2.7234339474441143·10^{1}	-2.1897653262707397·10^{1}	5.1788505812259071·10^{-2}
11	-1.8817843873687068·10^{3}	4.3038072285882070	6.6244087689671860·10^{-3}	-2.7133073605696295·10^{3}	-1.7951557394285043·10^{-5}
12	-1.7668827539244447·10^{2}	4.8160932330629913·10^{-1}	-6.3133007671100293·10^{-4}	2.5631774669873157·10^{4}	4.1534484127873519·10^{-7}
13	-1.6661835889222382·10^{3}	1.3708900504682877·10^{3}	-1.7919060052198969·10^{1}	-3.5145029804436405·10^{1}	5.1047240947371224·10^{-2}
14	1.0843549363030939·10^{4}	-7.3557073636139577·10^{1}	1.2054625131778862	1.9358737917864391·10^{2}	-4.2871620775911338·10^{-3}
15	-2.4269802549752835·10^{3}	1.1348265061941714·10^{1}	-5.0430423939495157·10^{-2}	2.3709874548950634·10^{3}	1.4091851828620244·10^{-4}
16	5.2745372575251588·10^{2}	-2.6080675912627314	5.6902218056670145·10^{-3}	-3.2149319482897838·10^{4}	-5.4121996056745853·10^{-6}
17	-1.6401959518360403·10^{1}	2.4322962162439640·10^{-1}	1.1744366627725344·10^{-3}	-8.2694427518413195·10^{3}	-5.0028379203873102·10^{-6}
18	-2.7556572017167782·10^{3}	4.9293344495058264·10^{1}	-2.6503456520676050·10^{-1}	1.2130698030982167·10^{3}	4.3530610668042957·10^{-4}
19	-6.3419182228959192	4.0636212834605827·10^{-2}	-1.0450112687842742·10^{-4}	3.1035882189759656·10^{2}	9.4328418657873500·10^{-8}
20	3.0189213304689042·10^{3}	-2.3804654203861684·10^{1}	6.8113013411972942·10^{-2}	6.3112071081188913·10^{2}	-9.4460854261685723·10^{-5}
21	1.1924791930673702·10^{4}	-1.1973824959206000·10^{2}	1.6888713097971020·10^{-1}	1.8735938211539585·10^{2}	5.0974564680442852·10^{-4}
22	3.6409071302482083·10^{1}	1.7919859306449623·10^{-1}	-1.0020116255895206·10^{-3}	-8.3521083354432303·10^{3}	1.5879900546795635·10^{-6}

Table 3. Coefficients $c_{1-4,N}$ of the Eq. (18).

N	$c_{1,N}$	$c_{2,N}$	$c_{3,N}$	$c_{4,N}$
1	-3.6318550637865524·10^{-8}	2.1740704135789128·10^{-9}	-8.5521429066506161·10^{-12}	-9.3538647454573390·10^{-15}
2	2.1366936839394922·10^{-8}	-2.4087168827395623·10^{-10}	8.7969869277074319·10^{-13}	-1.0294466881303291·10^{-15}
3	-7.7804007761164303·10^{-10}	1.0327058173517932·10^{-11}	-4.2557697639692428·10^{-14}	5.4082507061618662·10^{-17}
4	3.2628927397420860·10^{-12}	-7.6475692919751066·10^{-14}	4.1985816845259788·10^{-16}	-6.2281395889592719·10^{-19}
5	2.0442205540818555·10^{-9}	4.0441858911249830·10^{-8}	-3.3423487629482825·10^{-10}	6.8000404742985678·10^{-13}
6	1.8381489183824627·10^{-8}	-8.9853322951518919·10^{-9}	7.5888799566036185·10^{-11}	-1.5823457864755549·10^{-13}
7	1.1795760639695057·10^{-7}	-8.1046722896375875·10^{-10}	9.1868604369041857·10^{-14}	4.7882428237444610·10^{-15}
8	-4.4028846582545952·10^{-9}	4.6541269232626618·10^{-11}	-1.1939929984285194·10^{-13}	2.3602037016614437·10^{-17}
9	2.7885056884209128·10^{-11}	-4.5167129624119121·10^{-13}	1.6558404997394422·10^{-15}	-1.2037336621218054·10^{-18}
10	-2.3719627171699983·10^{-9}	-1.5260127909292053·10^{-7}	1.7177017944754134·10^{-9}	-4.7031737537526395·10^{-12}
11	-5.6946433724699646·10^{-9}	8.4629788237081735·10^{-9}	-1.7674135187061521·10^{-10}	6.6236547903091862·10^{-13}
12	-2.2808617930606012·10^{-8}	1.4773376696847775·10^{-10}	-1.3076953119957355·10^{-13}	2.3625301497914000·10^{-16}
13	1.4014269939947841·10^{-10}	-2.3675117757377632·10^{-12}	5.1514033966707879·10^{-15}	-4.8864233454747856·10^{-18}
14	6.5464943868885886·10^{-11}	1.6494354816942769·10^{-8}	-1.7480097393483653·10^{-10}	4.7460075628523984·10^{-13}
15	8.4737893183927871·10^{-9}	-6.0243327445597118·10^{-9}	5.8766070529814883·10^{-11}	-1.4926748560042018·10^{-13}
16	1.0761964135701397·10^{-7}	-1.0142496009071148·10^{-9}	2.1337312466519190·10^{-12}	1.6376014957685404·10^{-15}
17	-3.5621571395968670·10^{-9}	4.1175339587760905·10^{-11}	-1.3535372357998504·10^{-13}	8.9334219536920720·10^{-17}
18	2.0700482083136289·10^{-11}	-3.9238944562717421·10^{-13}	1.5850961422040196·10^{-15}	-1.5336775610911665·10^{-18}
19	1.8524255464416206·10^{-9}	-2.1959816152743264·10^{-11}	-6.4478119501677012·10^{-14}	5.5135243833766056·10^{-16}
20	1.9349488650922679·10^{-9}	-2.2647295919976428·10^{-11}	9.2917479748268751·10^{-14}	-1.2741959892173170·10^{-16}
21	2.1484978031650972·10^{-11}	-9.3976642475838013·10^{-14}	-4.8892738002751923·10^{-16}	1.4676120441783832·10^{-18}
22	6.7565715216420310·10^{-13}	-3.5421162549480807·10^{-15}	-3.4201196868693569·10^{-18}	2.2260187650412392·10^{-20}

The sulfuric acid threshold concentration (in cm^{-3}) for kinetic ion-induced particle formation can be expressed as a function of temperature and relative humidity with

$$\begin{aligned}
\ln \rho_a^{\mathrm{kin}} \;=\;& 5.3742280876674478\cdot 10^{1} - 6.6837931590012266\cdot 10^{-3}\cdot\left[\ln(\frac{RH}{100})\right]^{-2} \\
& -1.0142598385422842\cdot 10^{-1}\cdot\left[\ln(\frac{RH}{100})\right]^{-1} - 6.4170597272606873\cdot\ln(\frac{RH}{100}) \\
& -6.4315798914824518\cdot 10^{-1}\cdot\left[\ln(\frac{RH}{100})\right]^{2} - 2.4428391714772721\cdot 10^{-2}\cdot\left[\ln(\frac{RH}{100})\right]^{3} \\
& -3.5356658734539019\cdot 10^{-4}\cdot\left[\ln(\frac{RH}{100})\right]^{4} + 2.5400015099140506\cdot 10^{-5}\cdot T\cdot\left[\ln(\frac{RH}{100})\right]^{-2} \\
& -2.7928900816637790\cdot 10^{-4}\cdot T\cdot\left[\ln(\frac{RH}{100})\right]^{-1} + 4.4108573484923690\cdot 10^{-2}\cdot T\cdot\ln(\frac{RH}{100}) \\
& +6.3943789012475532\cdot 10^{-3}\cdot T\cdot\left[\ln(\frac{RH}{100})\right]^{2} + 2.3164296174966580\cdot 10^{-4}\cdot T\cdot\left[\ln(\frac{RH}{100})\right]^{3} \\
& +3.0372070669934950\cdot 10^{-6}\cdot T\cdot\left[\ln(\frac{RH}{100})\right]^{4} + 3.8255873977423475\cdot 10^{-6}\cdot T^{2}\cdot\left[\ln(\frac{RH}{100})\right]^{-1} \\
& -1.2344793083561629\cdot 10^{-4}\cdot T^{2}\cdot\ln(\frac{RH}{100}) - 1.7959048869810192\cdot 10^{-5}\cdot T^{2}\cdot\left[\ln(\frac{RH}{100})\right]^{2} \\
& -3.2165622558722767\cdot 10^{-7}\cdot T^{2}\cdot\left[\ln(\frac{RH}{100})\right]^{3} - 4.7136923780988659\cdot 10^{-9}\cdot T^{3}\cdot\left[\ln(\frac{RH}{100})\right]^{-1} \\
& +1.1873317184482216\cdot 10^{-7}\cdot T^{3}\cdot\ln(\frac{RH}{100}) + 1.5685860354866621\cdot 10^{-8}\cdot T^{3}\cdot\left[\ln(\frac{RH}{100})\right]^{2} \\
& -1.4329645891059557\cdot 10^{4}\cdot T^{-1} + 1.3842599842575321\cdot 10^{-1}\cdot T \\
& -4.1376265912842938\cdot 10^{-4}\cdot T^{2} + 3.9147639775826004\cdot 10^{-7}\cdot T^{3}.
\end{aligned} \tag{19}$$

In the kinetic range the ion-induced particle formation can be described with the following equation [*Merikanto et al.,* 2015]:

$$J_{\mathrm{kin,ion-induced}} = C\rho_{\mathrm{pre}}\sqrt{T}(\rho_a^{\mathrm{total}}) \tag{20}$$

where C is given as in Eq. 12 with $r_{\mathrm{ref}} = r_{\mathrm{ion}} = 0.487\cdot 10^{-9}$m and $m_{\mathrm{ref}} = m_{\mathrm{ion}} = 1.661\cdot 10^{-27}$kg, and the pre-existing cluster concentration ρ_{pre} is simply the negative ion concentration ρ_{ion}.

4.3 How to apply the parameterizations in practice?

For simplifying the use of the parameterizations, we are distributing Fortran codes in the Supplementary Materials of this article. The following points should be kept in mind when using the parameterizations.

1. The total particle formation rate is the sum of neutral and ion-induced cases: $J_{\mathrm{tot}} = J_{\mathrm{neutral}} + J_{\mathrm{ion}}$.

335 **Table 4.** List of the parameterizations developed in this article.

Parameterization	Neutral	Ion-induced
Kinetic threshold $\rho_a^{\mathrm{kin}}[1/\mathrm{cm}^3]$	Eqs. (8), (9), (10)	Eq. (19)
x	Eq. (1)	Eq. (1)
J_{nuc}	Eq. (2)	Eqs. (13), (14), Table 1
N_{tot}	Eq. (3)	Eqs. (15), (16), Table 2
r	Eq. (4)	Eqs. (17), (18), Table 3
Threshold $\rho_a^{J=1}[1/\mathrm{cm}^3]$	Eqs. (5), (6), (7)	–

321 2. The ion-induced formation rate is limited by the ion pair production rate (I.P.R.): $J_{\mathrm{ion}} =$
322 $\min(J_{\mathrm{ion}}, I.P.R.)$.
323 3. The ion-induced particle formation rate is directly proportional to the negative ion con-
324 centration: $J_{\mathrm{ion}} \propto N_{\mathrm{ion}}$. The parameterization has been generated for $N_{\mathrm{ion}} = 1$ cm^{-3}
325 and should be scaled accordingly.
326 4. The particle formation rates are calculated at the (critical) formation size. If the param-
327 eterizations are used in comparison with measurements at larger sizes or in an atmo-
328 spheric model where the smallest size bin is larger than the formation size, the forma-
329 tion rates at those sizes should be evaluated using formulations developed for this pur-
330 pose [*Kerminen and Kulmala*, 2002; *Lehtinen et al.*, 2007]. For example, to calculate
331 the formation rates at the size of 3 nm: $J_{3\mathrm{nm}} = J_{\mathrm{neutral}} \cdot KK(r^*_{\mathrm{neutral}}) + J_{\mathrm{ion}} \cdot KK(r^*_{\mathrm{ion}})$,
332 where KK is the scaling given by, for example, *Kerminen and Kulmala* [2002] or *Lehti-*
333 *nen et al.* [2007].

334 Finally, we provide a quick reference of the different parameterizations in Table 4.

336 5 Results

337 In this section, we compare the new theoretical particle formation rates [*Merikanto et al.*,
338 2015] against the old [*Vehkamäki et al.*, 2002] and new parameterized particle formation rates
339 and cluster properties in a wide range of conditions.

340 Furthermore, to test the parameterization in realistic atmospheric modeling conditions,
341 we have also implemented the new neutral particle formation parameterization in the global

aerosol-climate model ECHAM5.5-HAM2 [*Stier et al.*, 2005; *Zhang et al.*, 2012]. This model describes the aerosol population with four soluble and three insoluble log-normal modes, including sulfate, organic carbon, black carbon, dust and sea salt. The simulations start in June 1999 with a 6-month spin-up period and end in December 2000: analysis is done only for year 2000. The model is nudged against ERA-40 meteorology to improve signal-to-noise ratio. The simulations include anthropogenic aerosol and precursor emissions from ACCMIP [*Lamarque et al.*, 2010], while sea salt, dust and DMS emissions are calculated online. We apply the model in two cases, 1) with the default *Vehkamäki et al.* [2002] binary nucleation parameterization and 2) with the new parameterization, and we will present this comparison as well.

5.1 Neutral parameterization

Figures 1, 2, 3 and 4 show a comparison of the theoretical and the parametrized values for particle formation rate, sulfuric acid mole fraction, total number of molecules and radius of the critical cluster, respectively.

The ratio of the theoretical and the parameterized particle formation rates (Fig. 1) shows that in the whole range of particle formation rates most of the cases are within one order of magnitude (10^{-1}–10^{1}) of the perfect fit. Our wider ranges for all the input variables cause larger deviations between the theoretical values and the fit than in the parametrization of *Vehkamäki et al.* [2002]. For very low and very high theoretical particle formation rates the parameterization may overestimate the rates by a factor of 10^3 in some cases. These cases are related to the extremities of the validity ranges. For example, for high sulfuric acid concentrations (above 10^9 cm^{-3}) sometimes the model predicts very large clusters (n_{tot} around 100) with corresponding very low particle formation rates, which are overestimated by the parameterization. This overestimation grows with growing sulfuric acid concentration and is particularly clear for concentrations above approximately 10^{11} cm^{-3}, giving the highest overestimations of small particle formation rates (cases on the left extremity of Fig. 1 for $J_{\mathrm{theoretical}}/J_{\mathrm{param}}$ values below 10^{-2}). However, the largest discrepancies between the theoretical and the parameterized particle formation rates are either at insignificantly low particle formation rates, where the particle formation is practically zero, or at extremely high particle formation rates where particle formation rate is not the limiting factor for appearance of particles of atmospheric relevance, but also growth and loss processes play a major role.

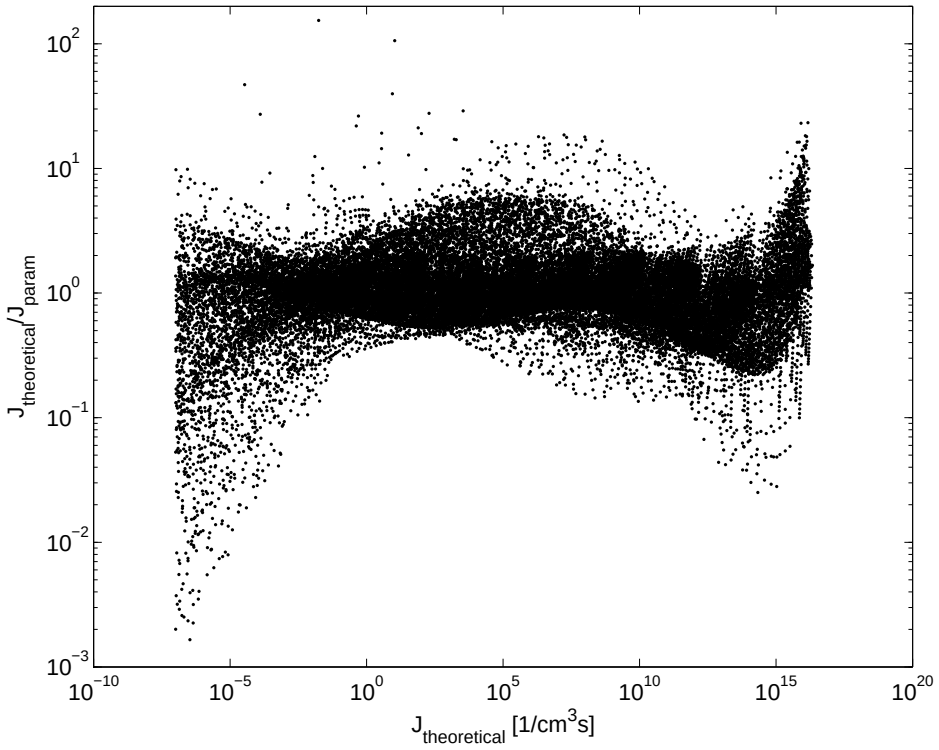

355 **Figure 1.** Comparison between the parameterized and the theoretical values for the neutral particle forma-

356 tion rate J_{neutral}.

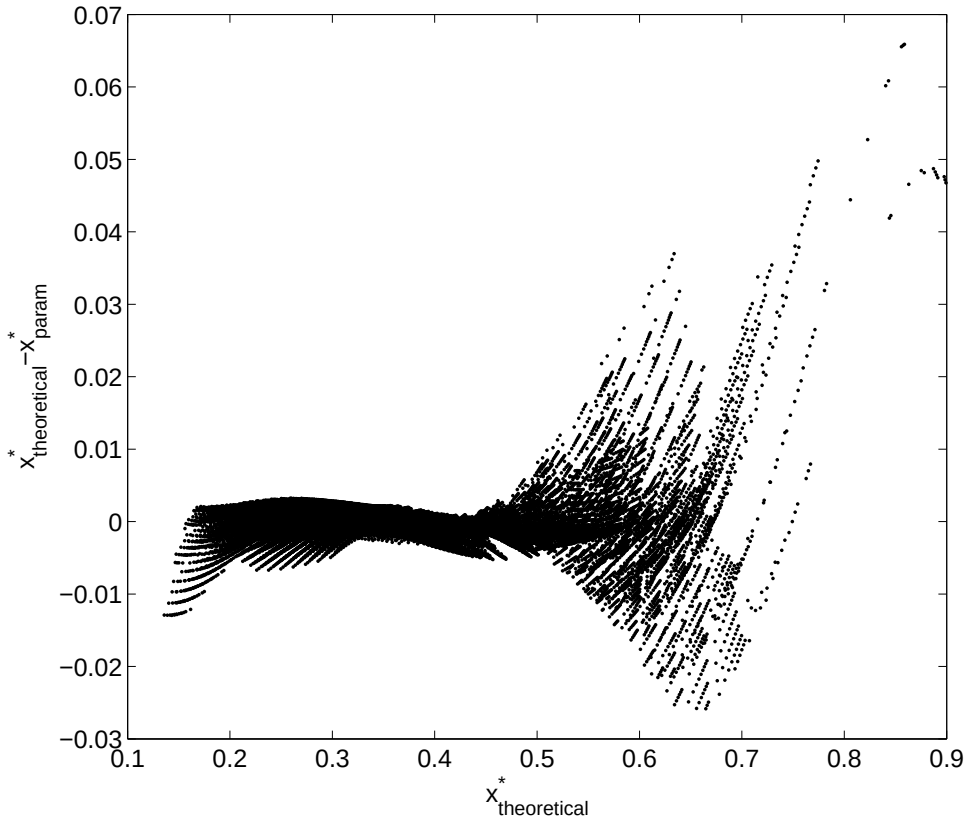

Figure 2. Comparison between the parameterized and the theoretical values for the critical cluster mole fraction x^* in the neutral case.

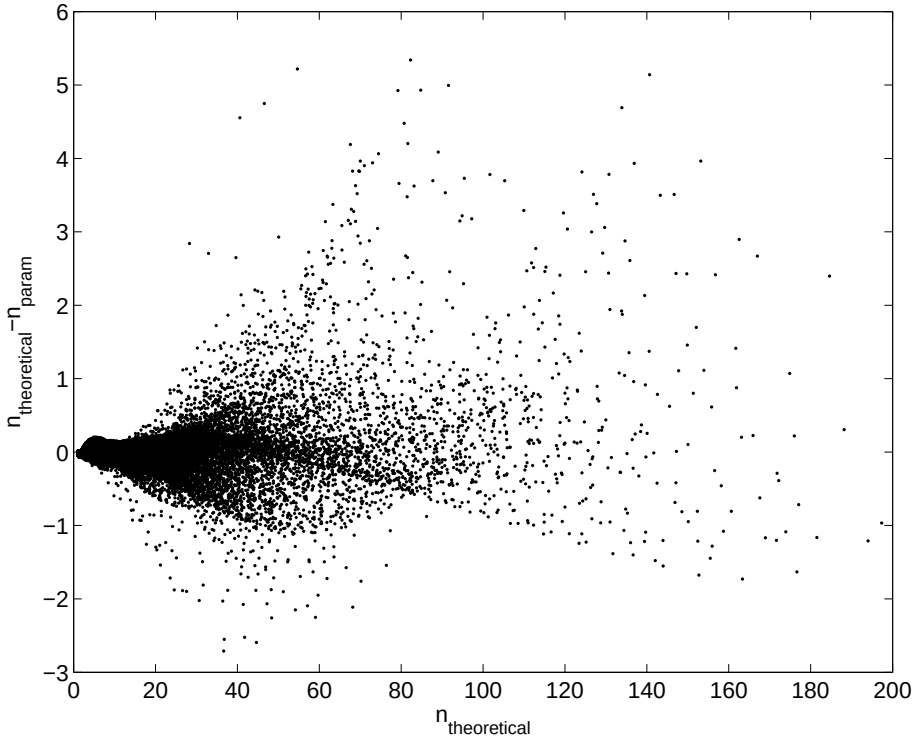

359 **Figure 3.** Comparison between the parameterized and the theoretical values for the total number of
360 molecules in the critical cluster $n^*_{\rm tot}$ in the neutral case.

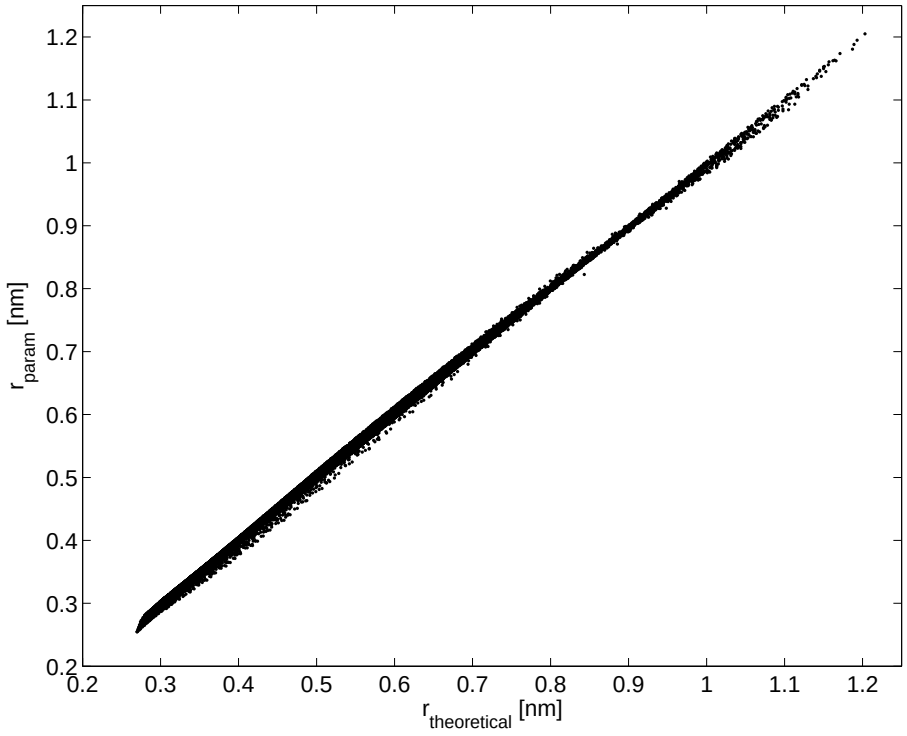

Figure 4. Comparison between the parameterized and the theoretical values for the critical cluster radius r^* in the neutral case.

Figure 2 shows the difference between the theoretical and parameterized mole fractions. Fractions below x <0.5 are best fitted (difference between theory and parameterization ranging between -0.017 and 0.007), but above this value the difference grows. In particular, the mole fractions above x >0.7 are somewhat overestimated (deviation up to 0.069) by the parameterization. The relative errors are at most around 13% (lowest mole fractions) and stay below 9% at high mole fractions. The best fits are acquired in the range $x = 0.33 - 0.45$ (relative errors around or less than 1%).

The difference between the theoretical and the parameterized total number of molecules n_{tot} in the critical cluster seen in Fig. 3 shows a best fit for small n_{tot} with larger absolute deviations appearing the larger the n_{tot} is. The values of n_{tot} vary from 1 to 200, with the large total numbers corresponding to very small particle formation rates, with a lower limit of J=10^{-7}cm^{-3}s^{-1}. The deviations range between -3 and +5 molecules at n_{tot}=40 and n_{tot}=55, respectively, giving a relative error of less than 10 %.

The critical cluster radii vary approximately between 0.28 nm and 1.2 nm (Fig. 4) with the ratio of the theoretical and the parameterized radii ranging between 0.98 and 1.07.

Figure 5 shows the behavior of the particle formation rate for several sulfuric acid concentrations as a function of temperature and relative humidity. It can be seen that the difference between the *Vehkamäki et al*. [2002] model (crosses) and parameterization (dashed lines) and the present model (triangles) and parameterization (solid lines) is largest at low temperatures and at low relative humidities. The old and present particle formation rates are nearly superposed above 230-250 K and above RH=1% of relative humidity (see the lowest four panels of Fig. 5), but differences are seen already at 270 K when RH<1% and at 240K with RH<10%, depending also on the acid concentration. The largest differences between the present and *Vehkamäki et al.* [2002] results are seen at low acid concentrations (top panels in Fig. 5). The old parameterization is not valid below 190K (absence of dashed lines). The difference between the old and new models is also large at low relative humidities RH<1%, depending also on the acid concentration. Similarly, in the upper left panel of Fig. 5 the particle formation rates are seen to differ the most below 210 K and particularly so for low relative humidities. Figure 5 demonstrates the good quality of our new parameterization, since the solid lines (the parameterized particle formation rates) are well superposed with the triangles representing the theoretical results. Comparison of the dashed and solid lines in the plots also reveals the larger validity range of the new parameterization. Note in particular the kinetic range (black lines and triangles),

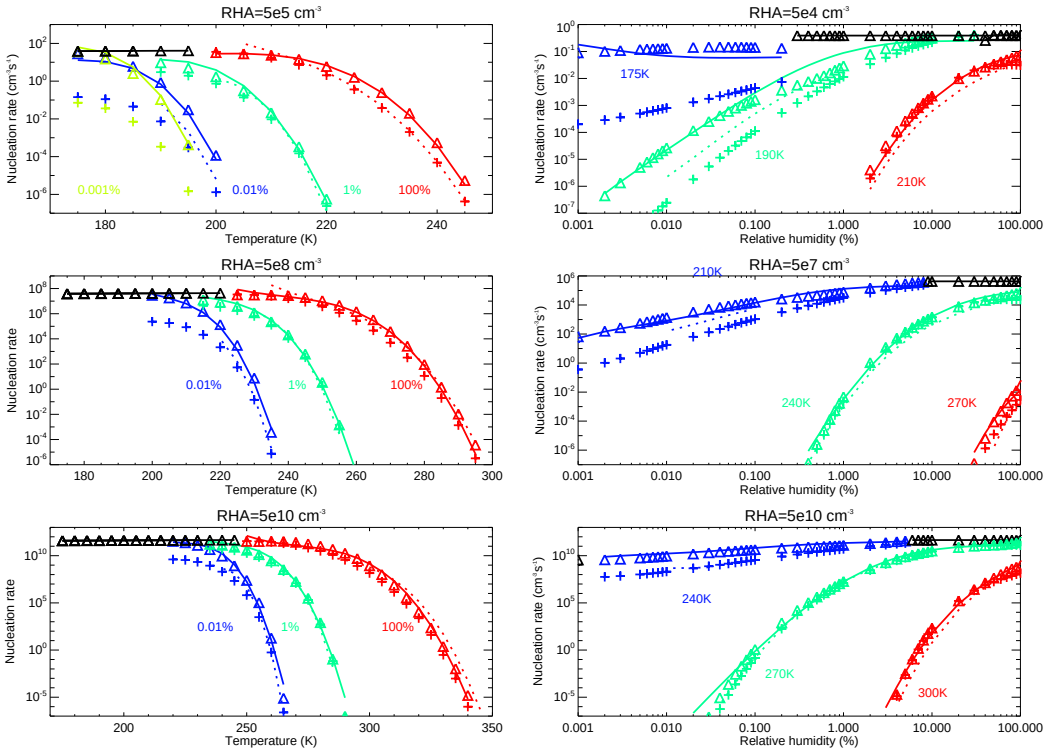

Figure 5. Left: The neutral particle formation rate J as a function of temperature at different total sulfuric acid concentrations and relative humidities. The relative humidities correspond to different colors as marked in the plot. Right: The particle formation rate as a function of relative humidity at different total sulfuric acid concentrations and temperatures. The temperatures correspond to different colors as marked in the plot. The sulfuric acid concentrations (RHA=ρ_a) are given in the plot titles [1/cm^3]. The crosses and dashed lines show, respectively, the old theoretical values and the old parameterization [*Vehkamäki et al.*, 2002]. The triangles and solid lines show, respectively, the new theoretical values and the new parameterized rates. The black triangles and solid lines show the kinetic particle formation rates calculated with Eqs. (11) and (12).

now accessible with our parameterization. A slight discontinuity can be seen on the upper right panel at 175 K, with the parameterization (solid lines) exhibiting a dip just before arriving at the kinetic limit. This is due to difficulties in fitting the functional form of the parameterization at the edge of the validity range.

Figure 6 shows the behavior of the threshold concentration parameterization. The ratio of the theoretical to the parameterized values for the sulfuric acid concentration corresponding to particle formation rate 1 $cm^{-3}s^{-1}$ is 0.99-1.01 in the temperature range 155-185 K (kinetic range), 0.92-1.16 in the range 190-310 K and 0.83-1.13 in the range 310-400 K. It can be seen that at all but the lowest temperatures, as expected, the required sulfuric acid concentration decreases with decreasing temperature. For a given acid concentration, the saturation vapor pressure decreases and thus the saturation ratio increases with decreasing temperature. This leads to a lower particle formation barrier, and a larger value for the exponential term in the particle formation rate equation. At the same time the particle formation kinetics slows down, but the growth of the exponential term dominates. However, we can see that this is valid only down to temperature of 190 K (see Fig. 7), around which the kinetic regime is entered. Below this, the necessary acid concentration starts to increase with decreasing temperature. This can be explained by the vanishing particle formation barrier, leaving the kinetics as the determining factor. Since the kinetic processes slow down with decreasing temperature, a higher acid concentration will be required to maintain the same particle formation rate. This behavior was not seen in *Vehkamäki et al.* [2002], since they limited their cluster sizes to $n_{\mathrm{tot}} > 4$, whereas we go down to $n_{\mathrm{tot}} > 1$, and also model specifically the kinetic range. Note that in Fig. 7 the data points behave in a step-like manner only because of the coarse resolution of the sulfuric acid concentration grid.

The kinetic limit is described as the threshold sulfuric acid concentration above which particle formation is kinetic at a certain relative humidity and temperature. This concentration is lowest at low temperatures: for example, it is between 10^0 and 10^4 cm^{-3} at 160 K. The variation of the threshold concentration for a constant temperature arises from the RH-dependence, giving the lowest threshold at highest RH. The kinetic threshold concentration increases towards higher temperatures reaching 10^{18} cm^{-3} at 400 K. The fit for the sulfuric acid concentration at the kinetic limit is within 10-12% of the theoretical results. The absolute lowest RH data value used is $5{\cdot}10^{-6}$, but the minimum RH value depends on the temperature. Note that RH=0% can not be used because the fitting function contains logarithms of RH.

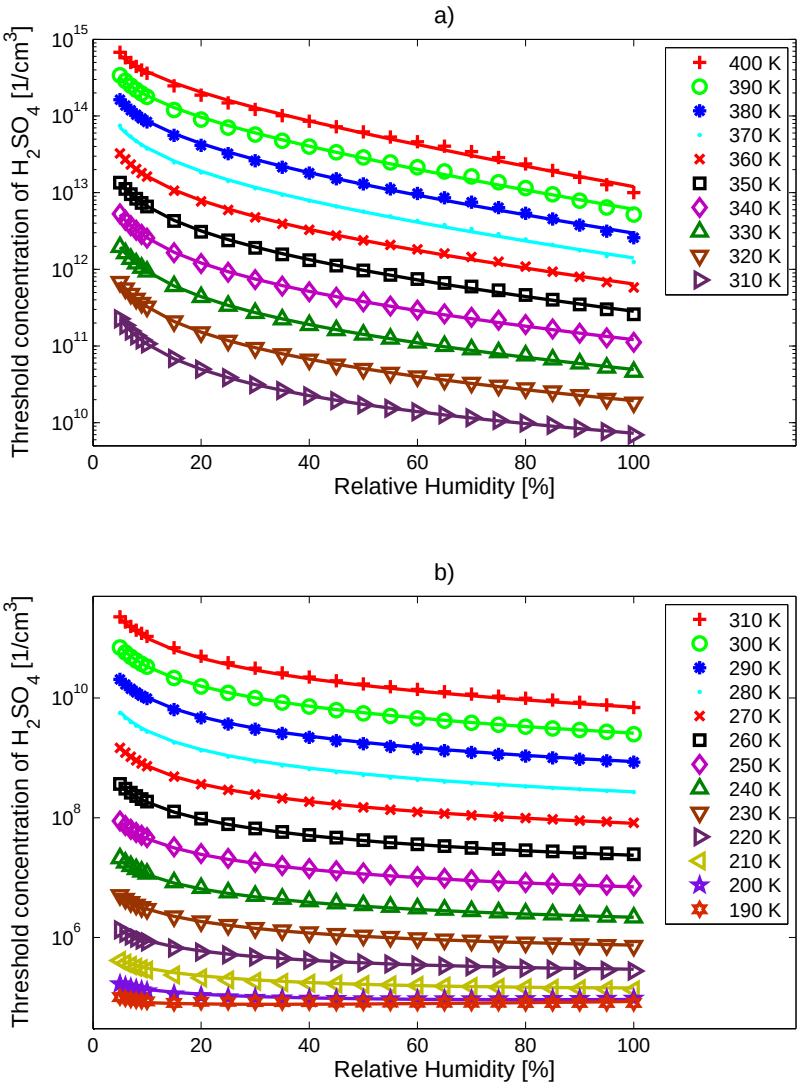

Figure 6. The threshold sulfuric acid concentration parameterization (lines, data with symbols) yielding neutral particle formation rates 1 $cm^{-3}s^{-1}$ as function of relative humidity. Upper panel: temperature range from 310 K to 400 K. Lower panel: 190-310 K. The temperatures are as given in the legend.

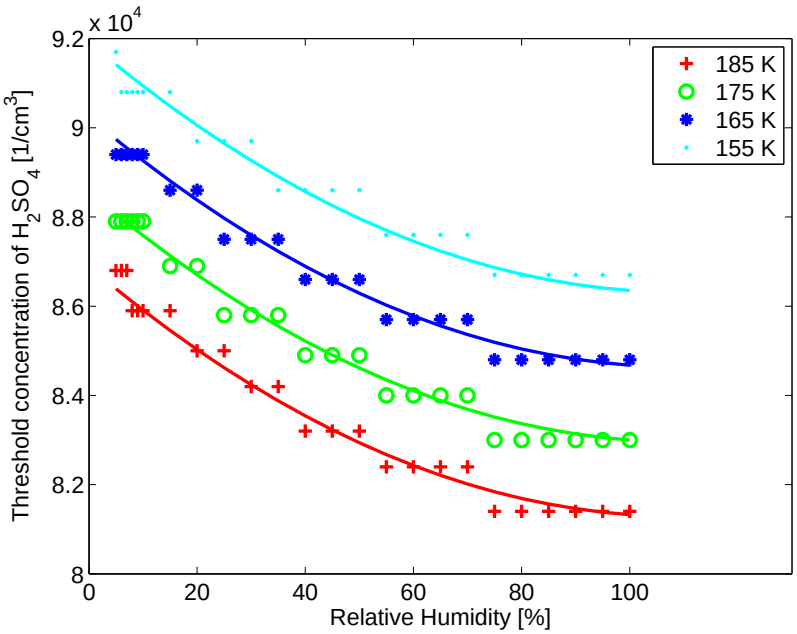

Figure 7. The threshold sulfuric acid concentration parameterization (lines, data with symbols) yielding neutral particle formation rates 1 $cm^{-3}s^{-1}$ in the kinetic range, at temperatures ranging from 155 K to 185 K. The step-wise behavior of the data points is only an artifact of the sulfuric acid grid resolution we used for calculating the data.

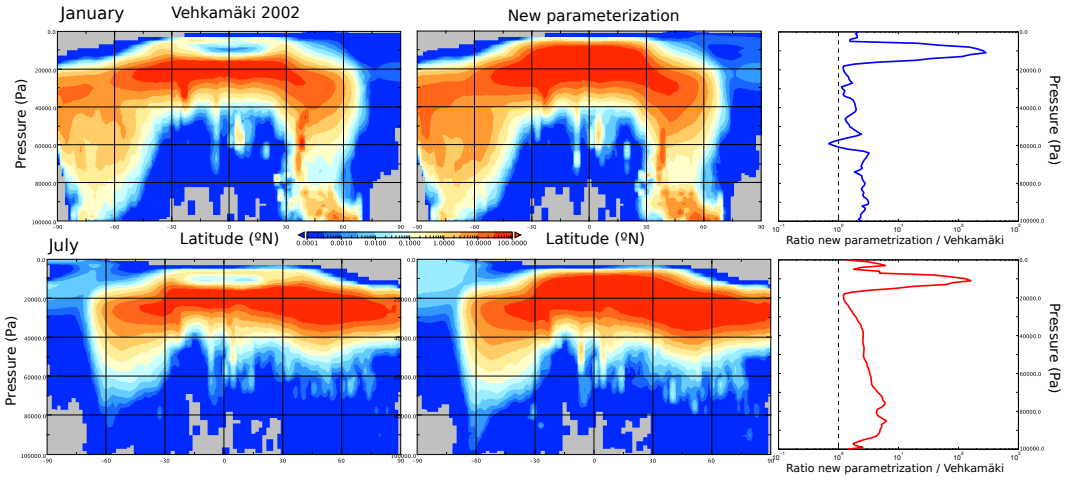

Figure 8. Results of the comparison of the old and new parameterizations within the ECHAM5.5-HAM2 model. The leftmost panels show zonal mean particle formation rates calculated with the *Vehkamäki et al.* [2002] parameterization and the middle panels the rates calculated with the new parameterization. The formation rates are presented as function of latitude and pressure. The rightmost panels show the ratio of the particle formation rates given by the new parameterization to the ones calculated with *Vehkamäki et al.* [2002]. The upper panels show results for January and the lower panels for July.

Figure 8 shows the ECHAM5.5-HAM2 model results of the comparison of particle formation rates calculated with the *Vehkamäki et al.* [2002] parameterization and the new one. Both *Vehkamäki et al.* [2002] and new parameterization produce an overall similar zonal pattern (Fig. 8) with high average nucleation rates of 10-100 cm^{-3} s^{-1} in the UTLS and generally low rates in the lower atmosphere, which is also found in earlier studies [*Makkonen et al.*, 2009; *Yu et al.*, 2010; *Lee et al.*, 2013]. During NH winter, nucleation rates up to 0.1-1 cm^{-3} s^{-1} can extend below 800 hPa between 30-70°N due to cold continental temperatures in Siberia and Northern America.

A gap in nucleation rate is visible in both January and July simulation with *Vehkamäki et al.* [2002] parameterization around 100 hPa between 15°S-15°N, since the parameterization was limited to critical clusters of at least 4 molecules. This gap has been filled in the simulations with new parameterization. Hence, the dominant effect of using the improved parameterization is seen as an increase of global nucleation rates by a factor of 100 around 100 hPa, thanks to the wider validity range of the new parameterization to smaller critical clusters ($n_{\mathrm{tot}} < 4$) down to the kinetic range ($n_{\mathrm{a}}^{*} < 1$). However, even lower atmosphere (800-1000 hPa) nucleation rates are increased by a factor of 2-3 (January) and 2-6 (July) with the new parameterization.

5.2 Ion-induced parameterization

Figures 9, 10 and 11 show a comparison of the theoretical and the parametrized values for particle formation rate, total number of molecules and radius of the critical cluster, respectively, in the ion-induced case.

Fig. 9 reveals that in general the parameterization describes well the ion-induced particle formation rate, but seems to overestimate the rate in particular at the lowest and the highest theoretical formation rates. In most of the range the parameterized rates are within two orders of magnitude of the perfect fit with some excursions up to 3-4 orders of magnitude (largest overestimation by the parameterization being $3{\cdot}10^{4}$ and largest underestimation $8{\cdot}10^{2}$).

The parameterization for the number of molecules in the critical cluster (Fig. 10) overestimates the values at most by about 40% and underestimates the values by almost 50% in the smallest cluster sizes in some isolated cases, but overall the differences are smaller.

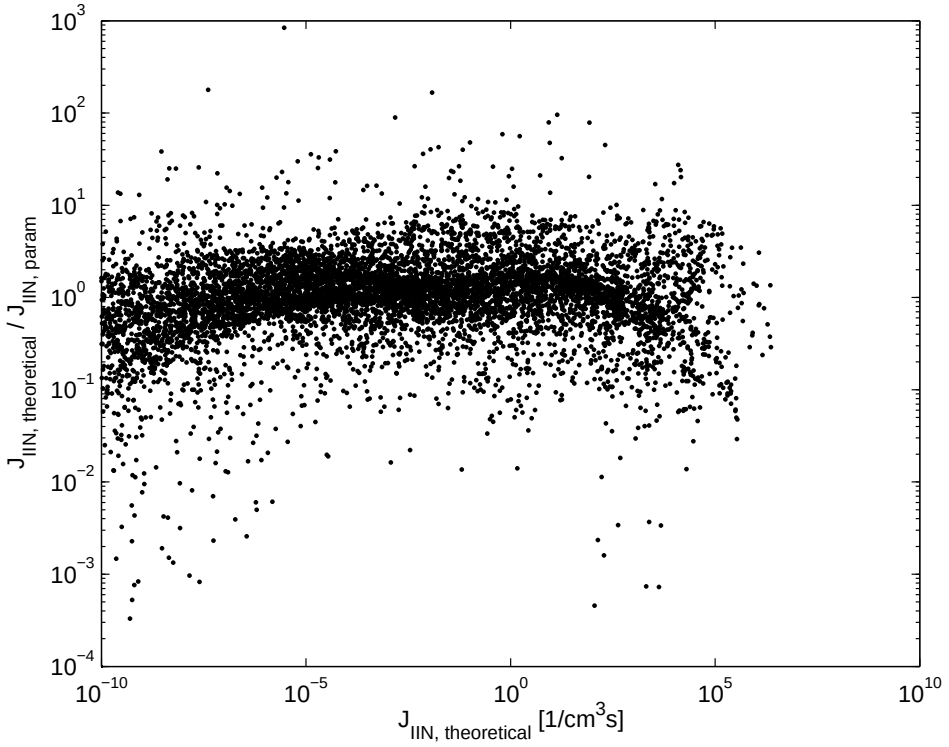

Figure 9. Comparison between the parameterized and the theoretical values for the ion-induced particle formation rate J_{ion}.

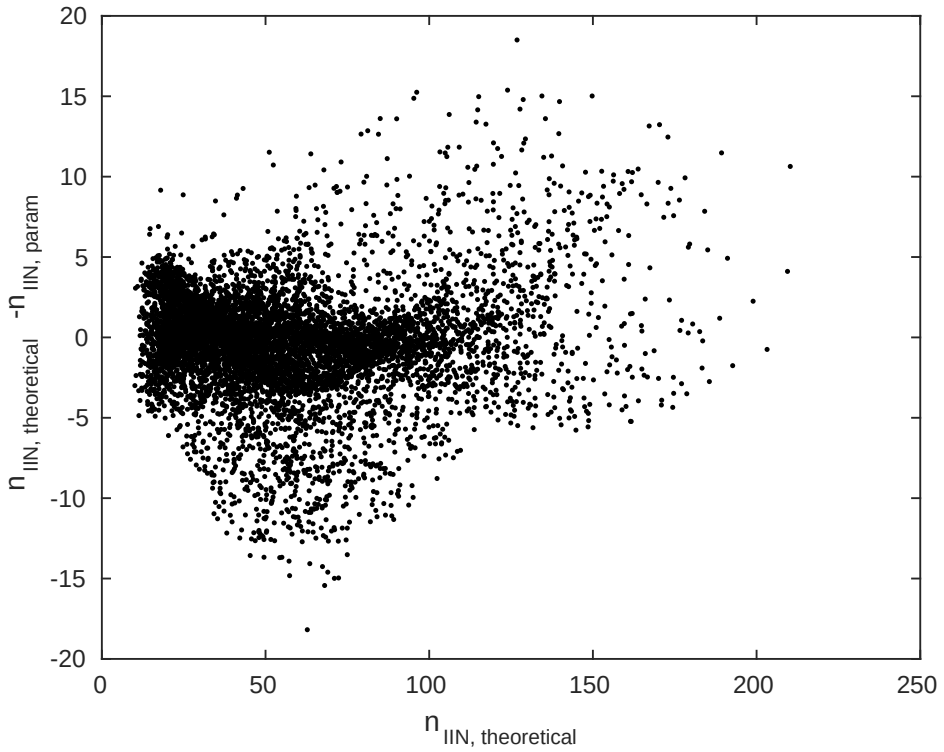

488 **Figure 10.** Comparison between the parameterized and the theoretical values for the total number of
489 molecules in the critical cluster n_{tot} in the ion-induced case.

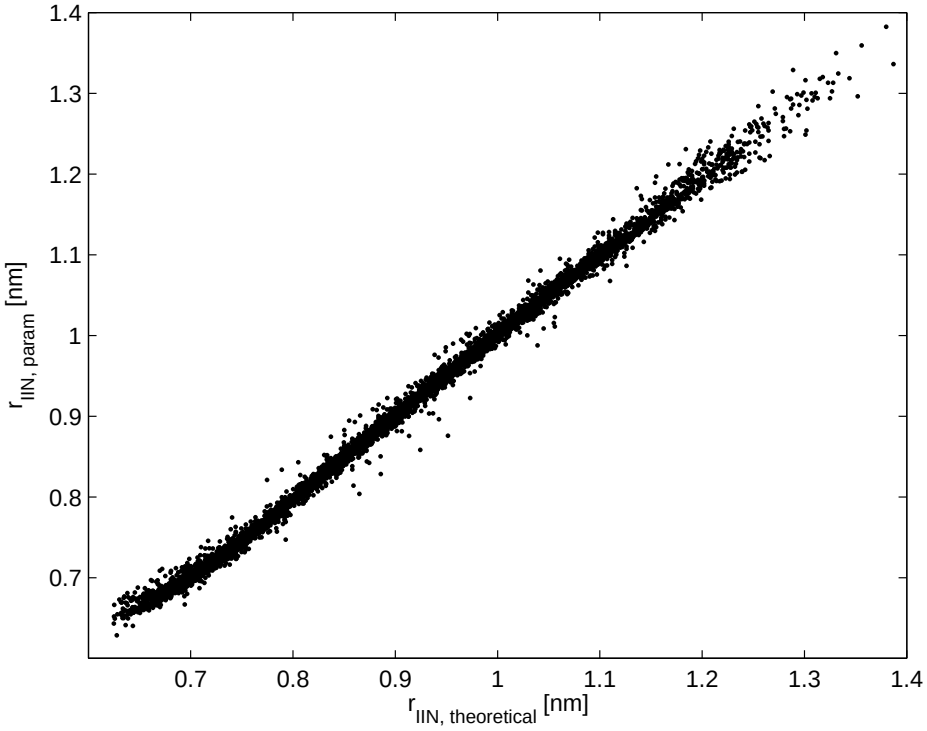

Figure 11. Comparison between the parameterized and the theoretical values for the critical cluster radius r^* in the ion-induced case.

The critical radius parameterization behaves well (Fig. 11) with slight overestimations of the radius at smallest sizes and underestimation at the largest sizes. The maximum deviations remain below 8%.

The parameterization for the sulfuric acid concentration at the kinetic limit is within 15% of the perfect fit most of the time, with highest values at the lowest and highest threshold concentration values. Naturally, as in the neutral case, the kinetic limit sulfuric acid concentration increases with increasing temperature and with decreasing relative humidity: the concentration is the highest at high temperatures and low relative humidities. The range of the kinetic limit sulfuric acid concentration spans a large range from 10^{-10}cm^{-3} at T=160 K and RH=100% to 10^{16}cm^{-3} at T=400 K and RH=0.1%. The concentrations are always significantly lower than the corresponding values for the neutral case.

Figure 12 shows a detailed comparison between the theoretical ion-induced particle formation rates (symbols) and the parameterized ones (lines). The kinetic range is shown in black. The ion-induced nucleation rate parameterization (solid lines) follows well the theory (triangles). The temperature at which the kinetic ion-induced range (black solid lines and triangles) is reached increases with increasing sulfuric acid concentration and increasing relative humidity, as for the neutral case.

6 Conclusions

We have developed new parameterizations based on an improved model [*Merikanto et al.*, 2015] for two-component particle formation of sulfuric acid and water in the neutral and ion-induced cases. The new neutral parameterization widens the validity range of the *Vehkamäki et al.* [2002] parameterization to lower relative humidities and higher sulfuric acid concentrations, and to a larger temperature range. Parameterizations are given for particle formation rate ($J >10^{-7}$ cm^{-3}s^{-1}), radius and composition of the critical cluster, and number of molecules ($n_{\rm tot} >1$) in the critical cluster. Above the sulfuric acid concentrations given by parameterized kinetic limit, a simple kinetic regime formula for the formation rate can be used. It should be noted that, as in *Vehkamäki et al.* [2002], the low temperature results are based on extrapolations of the thermodynamic parameters below 230 K.

The neutral parameterization for J deviates slightly more from the theoretical values than the one of *Vehkamäki et al.* [2002] but the largest discrepancies are found at very high or very low particle formation rates with little relevance for correctly predicting whether particle for-

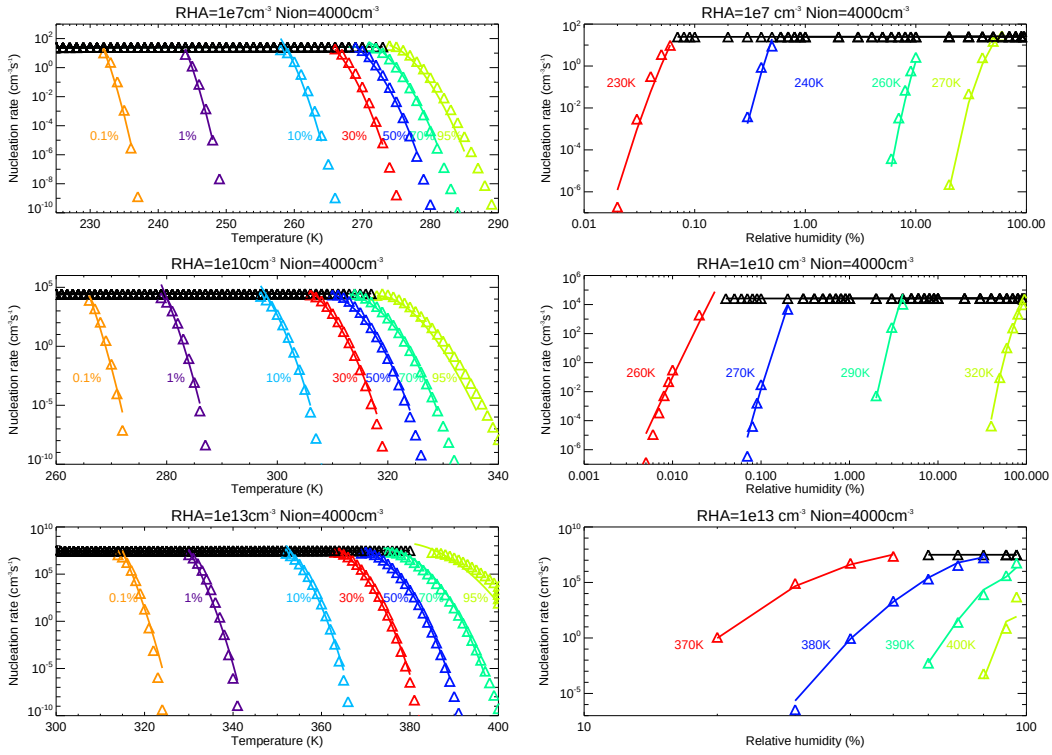

Figure 12. Left: The ion-induced particle formation rate J_{ion} as a function of temperature at different total sulfuric acid concentrations and relative humidities. The relative humidities correspond to the colors as marked in the plot. Right: The particle formation rate as a function of relative humidity at different total sulfuric acid concentrations and temperatures. The temperatures correspond to the colors as marked in the plot. The sulfuric acid concentrations (RHA=ρ_a) are given in the plot titles [1/cm^3]. The triangles and solid lines show, respectively, the theoretical values and the parameterization in the nucleation range. The black triangles and lines show, respectively, the kinetic range values calculated with Eq. (20).

mation is occurring or not. The other parametrized quantities follow the theoretical predictions well with errors mostly below 10% (12% at maximum). The new theory and the new parameterization differ the most from the ones of *Vehkamäki et al.* [2002] at low temperatures and relative humidities, and at low acid concentrations. We have also developed a parameterization for the threshold sulfuric acid concentration for $J = 1$ cm^{-3}s^{-1} and for the threshold sulfuric acid concentration above which particle formation is kinetic.

The ion-induced parameterization behaves overall as well as the neutral one, with the parameterization mainly overestimating by 3-4 orders of magnitude the particle formation rates at very low and high theoretical formation rates. For the critical cluster radius the relative differences are always below 8%, but for the number of molecules in the critical cluster the differences can reach almost 50%. The kinetic limit is well described by the parameterization, the relative difference being always below 15%.

We recommend using the new model and the improved parameterizations from now on instead of *Vehkamäki et al.* [2002]. The model performance has been compared to state-of-the-art particle formation measurements [*Duplissy et al.*, 2015]. The neutral parameterization widens the validity range of the *Vehkamäki et al.* [2002] parameterization, approaches correctly the one-component limit and the kinetic range limit has been parameterized as well. A new ion-induced parameterization has been produced for a large range of conditions, and it also includes the kinetic range limit. This development opens new opportunities for Terrestrial atmosphere studies, and also for the Venus cloud community, which can use the new parameterization in the range of conditions encountered within the Venus cloud formation region.

Fortran codes of the parameterizations are given in the Supplementary Material.

A: Behavior of the two-component nucleation theory at the one-component limit

When starting to develop the new parameterization, we were particularly interested in very low relative humidities, and preliminary calculations revealed formation of near-pure sulfuric acid clusters ($x \geq 0.99$) in these conditions. Thus we have performed both theoretical and numerical tests to ensure correct behavior of the two-component particle formation model at the one-component limit.

The general expression for nucleation rate J is

$$J = \frac{|\lambda_1|}{2\pi kT}\rho^* \frac{1}{\sqrt{|\det \frac{W^*}{2\pi kT}|}}, \tag{A.1}$$

where ρ^* is the number concentration of crtical clusters in the vapor phase. When using a self-consistent cluster distribution the concentration ρ^* known to reduce correctly to the one-component case at the one-component limit [*Wilemski and Wyslouzil*, 1995], but the behavior of the kinetic term $|\lambda_1|/\sqrt{|\det W^*|}$ needs to be examined, where $|\lambda_1|$ is the negative eigenvalue of the product matrix R^*W^*. The matrix R^* contains the condensation coefficients that describe the collisions of clusters of size n_a, n_w with the critical cluster:

$$R^*_{aa} = \sum_{n_a=1,n_w=0}^{N_c} n_a^2(r^*+r)^2\sqrt{8\pi kT\left(\frac{1}{m^*}+\frac{1}{m}\right)}\rho(n_a,n_w) \tag{A.2}$$

$$R^*_{ww} = \sum_{n_a=0,n_w=1}^{N_c} n_w^2(r^*+r)^2\sqrt{8\pi kT\left(\frac{1}{m^*}+\frac{1}{m}\right)}\rho(n_a,n_w) \tag{A.3}$$

$$R^*_{aw} = R^*_{wa} = \sum_{n_a=1,n_w=1}^{N_c} n_a n_w(r^*+r)^2\sqrt{8\pi kT\left(\frac{1}{m^*}+\frac{1}{m}\right)}\rho(n_a,n_w), \tag{A.4}$$

where N_c stands for the largest hydrate accounted for. The matrix W^* contains the second derivatives of the formation energy with respect to the number of molecules in the cluster (W_{aa},W_{aw},W_{ww}), which can be written as follows:

$$W_{aa} \equiv \frac{d^2\Delta\varphi}{dn_a^2} = \frac{-v_a(x^*)^2\sigma}{2\pi r^{*4}} + \left(kT\frac{d\mathcal{A}_a}{dx_a}\frac{1}{\mathcal{A}_a} + 2\frac{dv_a(x^*)}{dx_a}\frac{\sigma}{r^*} + 2v_a(x^*)\frac{d\sigma}{dx_a}\frac{1}{r^*}\right)\frac{n_w^*}{(n_a^*+n_w^*)^2} \tag{A.5}$$

$$W_{ww} \equiv \frac{d^2\Delta\varphi}{dn_w^2} = \frac{-v_w(x^*)^2\sigma}{2\pi r^{*4}} + \left(kT\frac{d\mathcal{A}_w}{dx_w}\frac{1}{\mathcal{A}_w} + 2\frac{dv_w(x^*)}{dx_w}\frac{\sigma}{r^*} + 2v_w(x^*)\frac{d\sigma}{dx_w}\frac{1}{r^*}\right)\frac{n_a^*}{(n_a^*+n_w^*)^2} \tag{A.6}$$

$$\begin{aligned} W_{aw} = W_{wa} \equiv \frac{d^2\Delta\varphi}{dn_w dn_a} \quad = \quad & \frac{-v_a(x^*)v_w(x^*)\sigma}{2\pi r^{*4}} + \left(kT\frac{d\mathcal{A}_w}{dx_w}\frac{1}{\mathcal{A}_w} + 2\frac{dv_w(x^*)}{dx_w}\frac{\sigma}{r^*}\right. \\ & \left. + 2v_w(x^*)\frac{d\sigma}{dx_w}\frac{1}{r^*}\right)\frac{n_w^*}{(n_a^*+n_w^*)^2} \end{aligned} \tag{A.7}$$

where $\mathcal{A}_a$ and $\mathcal{A}_w$ are, respectively, the gas phase activities of acid and water.

Here $\rho(n_a,n_w)$ is the concentration of clusters containing n_a sulfuric acid molecules and n_w water molecules, m^* and r^* are the mass and the radius of the critical cluster, and m and r are the mass and the radius of the cluster colliding with the critical cluster.

The eigenvalues $\lambda_{1,2}$ of the product matrix R^*W^*

$$\begin{pmatrix} R_{ww} & R_{wa} \\ R_{aw} & R_{aa} \end{pmatrix}\begin{pmatrix} W_{ww} & W_{wa} \\ W_{aw} & W_{aa} \end{pmatrix} \tag{A.8}$$

are

$$\lambda_{1,2} = \frac{1}{2}\left(\alpha \pm \sqrt{\alpha^2 - 4 \det R^* \det W^*}\right) \tag{A.9}$$

where we use the shorthand notation $\alpha = W_{ww}R_{ww} + W_{aa}R_{aa} + 2W_{wa}R_{wa}$. When the concentration of sulfuric acid, $\rho_a = \rho(1,0)$, is much higher than that of water, $\rho_w = \rho(0,1)$ (i.e., $\rho_a >> \rho_w$), the cluster consist almost solely of sulphuric acid, $x \geq 0.99$. The formation free energy surface around the critical cluster area forms a steep valley with almost vertical walls and the bottom of the valley running along the n_a-axis. When moving across the valley on a line parallel to the n_w-axis, the slope of the free energy surface changes fast from a large negative number to a large positive number when passing the critical size. Thus, magnitude of the second derivate $|W_{ww}|$ is large, approaching infinity for a truely one-component system. When moving along the bottom of the valley up to the critical size and down after that, the the slopes changes less rapidly, $|W_{ww}| >> |W_{aa}|$. Also, when comparing the almost infinite slopes in the n_w direction for different values of n_a, it can be concluded that these slopes do not depend strongly on the location along the n_a-axis, and thus $|W_{wa}|$ has a modest values and $|W_{ww}| >> |W_{wa}|$. Condensation coefficient R_{aa} contains terms representing the collisions of the critical cluster with small clusters with acid only, as well as those with both acid and water. If there is much more acid than water molecules in the systems, the acid only cluster dominate over the clusters with both acid and water molecules as well as over cluster with only water molecules. Coefficient R_{ww} contains terms representing with water clusters only and water-acid clusters, and coefficient R_{aw} contains terms representing only water-acid clusters, and thus it can be concluded that for nearly pure acid case $R_{aa} >> R_{wa}$, $R_{aa} >> R_{ww}$.

In this case the determinants of the matrices can be approximated as $\det W = W_{ww}W_{aa} - W_{wa}^2 \approx W_{ww}W_{aa}$ and $\det R = R_{ww}R_{aa} - R_{wa}^2 \approx R_{ww}R_{aa}$. Parameter α can be written as $\alpha = R_{ww}(W_{ww} + R_{aa}/R_{ww} \cdot W_{aa} + 2R_{wa}/R_{ww} \cdot W_{wa}) \approx W_{ww}R_{ww} + W_{aa}R_{aa}$. This is justified as R_{wa} and R_{ww} contain almost similar terms terms apart from the the term proportional to $\rho(0,1) = \rho_w$, which is very small compared to the terms corresponding to clusters with acid molecules in them. Another difference between R_{wa} and R_{ww} is the multiplication of the terms with $n_a n_w$ vs. multiplication with n_w^2, but this does not change the order of magnitude of the summation results. Thus R_{wa}/R_{ww} is of the order of 1, and $|W_{wa}|$ is small compared to $|W_{ww}|$, whereas R_{aa}/R_{ww} is large and thus $R_{aa}/R_{ww} \cdot W_{aa}$ can not safely be neglected although $|W_{ww}| >> |W_{aa}|$.

Inserting these approximations into Eq. (A.9) we get an approximate expression for the eigenvalues:

$$\lambda_{1,2} \approx \frac{1}{2}\left[W_{ww}R_{ww} + W_{aa}R_{aa} \pm (W_{ww}R_{ww} - W_{aa}R_{aa})\right]. \tag{A.10}$$

This results in simple expressions for the two eigenvalues of the product matrix R^*W^*

$$\lambda_{1,2} = \begin{cases} W_{aa}R_{aa} < 0 \\ \\ W_{ww}R_{ww} > 0. \end{cases} \tag{A.11}$$

and we can evaluate the term $|\lambda_1|/\sqrt{|\mathrm{detW}^*|}$ of the nucleation rate equation (A.1):

$$\frac{|\lambda_1|}{\sqrt{|\det W^*|}} \approx \frac{-W_{aa}R_{aa}}{\sqrt{|W_{ww}W_{aa}|}} = R_{aa}\sqrt{\frac{|W_{aa}|}{W_{ww}}}. \tag{A.12}$$

In the cases of two-component nucleation at the one-component limit we thus get:

$$J_{2-\mathrm{comp}}^{1-\mathrm{limit}} = R_{aa}\sqrt{\frac{|W_{aa}^{2-\mathrm{comp}}|}{W_{ww}^{2-\mathrm{comp}}}}\rho^* \tag{A.13}$$

since the $2\pi kT$ terms in equation (A1) cancel in the two-component case. The standard one-component Zeldovich factor reads [*Vehkamäki*, 2006]

$$J_{1-\mathrm{comp}} = R_{aa}\sqrt{\frac{|W_{aa}^{1-\mathrm{comp}}|}{2\pi kT}}\rho^*, \tag{A.14}$$

It can now be seen that

$$\frac{J_{2-\mathrm{comp}}^{1-\mathrm{limit}}}{J_{1-\mathrm{comp}}} = \sqrt{\frac{2\pi kT}{W_{ww}}}\sqrt{\frac{W_{aa}^{2-\mathrm{comp}}}{W_{aa}^{1-\mathrm{comp}}}}, \tag{A.15}$$

which indicates that the presence of water affects the nucleation rate even when approaching the only-acid limit.

This can be understood as follows: For numerical reasons the sulfuric acid mole fraction in the critical cluster can not be set to exactly one (in our study we used $x = 0.99$ at most), and as a consequence, water has necessarily a role in the process. Mathematically, in the hypothetical case of $x = 1$, some elements of matrices R^* and W^* would be zero or infinite and these matrices would thus be ill-behaved. In CNT the main contribution to the nucleation rate comes from the net flow of clusters through the critical cluster size in the direction of the eigenvector corresponding to the negative eigenvalue λ_1. The cluster flows on paths parallel to this main path, passing by the critical cluster size, are however taken into account by integrating over all these secondary paths giving rise to a factor $\sqrt{(2\pi kT/W_{ww})}$ seen in Eq. (A.15). As the second derivative W_{ww} does not approach $2\pi kT$ even though $\rho_a >> \rho_w$, this factor does not reduce to unity at the one-component limit. It must also be noted that because water concentration can not be equal to zero in the two-component theory, the second derivative W_{aa} does not exactly have its one-component value $v_a^2\sigma_a/(2\pi r^{*4})$ either.

Acknowledgments

We acknowledge the contribution of J. Julin for fitting the parameterization for the neutral particle formation. We are grateful for the IPSL Solar System Group that funded a one-week visit of Prof. Vehkamäki at the IPSL. We also acknowledge the ERC - Starting MOCAPAF grant no. 257360 and the Agence national de la recherche (ANR, project Exoclimats) for funding. JM and AM received a travel grant from Magnus Ehrnrooth foundation that helped immensely in finalizing this article.

References

Beig, G., and G. Brasseur (2000), Model of tropospheric ion composition: A first attempt, *J. Geophys. Res.*, *105*, 22,67122,684, doi:10.1029/2000JD900119.

Binder, K., and D. Stauffer (1976), Statistical theory of nucleation, condensation and coagulation, *Adv. Phys.*, *25*, 343–396.

Boucher, O., D. Randall, P. Artaxo, C. Bretherton, G. Feingold, P. Forster, V.-M. Kerminen, Y. Kondo, H. Liao, U. Lohmann, P. Rasch, S. Satheesh, S. Sherwood, B. Stevens, and X. Zhang (2013), *Climate Change 2013: The Physical Science Basis. Contribution of Working Group I to the Fifth Assessment Report of the Intergovernmental Panel on Climate Change*, chap. Clouds and Aerosols, Cambridge University Press, Cambridge, United Kingdom and New York, NY, USA.

Donald, W. A., , and E. R. Williams (2008), Evaluation of different implementations of the Thomson liquid drop model: Comparison to monovalent and divalent cluster ion experimental data, *The Journal of Physical Chemistry A*, *112*(16), 3515–3522, doi:10.1021/jp711012b, pMID: 18358015.

Donald, W. A., R. D. Leib, M. Demireva, B. Negru, D. M. Neumark, and E. R. Williams (2011), Average sequential water molecule binding enthalpies of $M(H_2O)_{19-124}{}^{2+}$ (M = Co, Fe, Mn, and Cu) measured with ultraviolet photodissociation at 193 and 248 nm, *The Journal of Physical Chemistry A*, *115*(1), 2–12, doi:10.1021/jp107547r.

Doyle, G. J. (1961), Self-Nucleation in the Sulfuric Acid-Water System, *J. Chem. Phys.*, *35*, 795–799, doi:10.1063/1.1701218.

Duplissy, J., J. Merikanto, A. Franchin, G. Tsagkogeorgas, J. Kangasluoma, D. Wimmer, H. Vuollekoski, S. Schobesberger, K. Lehtipalo, R. Flagan, D. Brus, N. Donahue, H. Vehkamäki, J. Almeida, A. Amorim, P. Barmet, F. Bianchi, M. Breitenlechner, E. Dunne, R. Guida, H. Henschel, H. Junninen, J. Kirkby, A. Kürten, A. Kupc,

A. Määttänen, V. Makhmutov, S. Mathot, T. Nieminen, A. Onnela, A. Praplan, F. Riccobono, L. Rondo, G. Steiner, A. Tome, H. Walther, U. Baltensperger, K. Carslaw, J. Dommen, A. Hansel, T. Petäjä, M. Sipilä, F. Stratmann, A. Vrtala, P. Wagner, D. Worsnop, J. Curtius, and M. Kulmala (2016), Effect of ions on sulfuric acid-water binary particle formation ii: Experimental data and comparison with qc-normalized classical nucleation theory, *J. Geophys. Res.*, pp. 1752–1775, doi:10.1002/2015JD023539, 2015JD023539.

Ehn, M., H. Junninen, T. Petäjä, T. Kurtén, V.-M. Kerminen, S. Schobesberger, H. E. Manninen, I. K. Ortega, H. Vehkamäki, M. Kulmala, and D. R. Worsnop (2010), Composition and temporal behavior of ambient ions in the boreal forest, *Atmos. Chem. Phys.*, *10*, 8513–8530.

Esposito, L. W., R. G. Knollenberg, M. I. Marov, O. B. Toon, and R. P. Turco (1983), The clouds and hazes of Venus, in *Venus*, edited by D. M. Hunten, L. Colin, T. M. Donahue, and V. I. Moroz, pp. 484–564, University of Arizona Press.

Gao, P., X. Zhang, D. Crisp, C. G. Bardeen, and Y. L. Yung (2014), Bimodal distribution of sulfuric acid aerosols in the upper haze of Venus, *Icarus*, *231*, 83–98, doi:10.1016/j.icarus.2013.10.013.

Henschel, H., J. C. A. Navarro, T. Yli-Juuti, O. Kupiainen-Määttä, T. Olenius, I. K. O. Colomer, S. L. Clegg, T. Kurtén, I. Riipinen, and H. Vehkamäki (2014), Hydration of atmospherically relevant molecular clusters: Computational chemistry and classical thermodynamics, *J. Phys. Chem. A*, *118*, 25992611.

Hirsikko, A., T. Nieminen, S. Gagné, K. Lehtipalo, H. E. Manninen, M. Ehn, U. Horrak, V.-M. Kerminen, L. Laakso, P. H. McMurry, A. Mirme, S. Mirme, T. Petäjä, H. Tammet, V. Vakkari, M. Vana, , and M. Kulmala (2011), Atmospheric ions and nucleation: a review of observations, *Atmos. Chem. Phys.*, *11*, 767798.

Hofmann, D., J. Barnes, M. O'Neill, M. Trudeau, and R. Neely (2009), Increase in background stratospheric aerosol observed with lidar at Mauna Loa Observatory and Boulder, Colorado, *Geophys. Res. Lett.*, *36*, L15808, doi:10.1029/2009GL039008.

Hommel, R., C. Timmreck, M. A. Giorgetta, and H. F. Graf (2015), Quasi-biennial oscillation of the tropical stratospheric aerosol layer, *Atmospheric Chemistry and Physics*, *15*(10), 5557–5584, doi:10.5194/acp-15-5557-2015.

James, E. P., O. B. Toon, and G. Schubert (1997), A numerical microphysical model of the condensational Venus cloud, *Icarus*, *129*, 147–171.

690 Kazil, J., and E. R. Lovejoy (2007), A semi-analytical method for calculating rates of new
691 sulfate aerosol formation from the gas phase, *Atmospheric Chemistry and Physics*, *7*,
692 3447–3459.

693 Kerminen, V.-M., and M. Kulmala (2002), Analytical formulae connecting the ”real” and
694 the ”apparent” nucleation rate and the nuclei number concentration for atmospheric
695 nucleation events, *JOURNAL OF AEROSOL SCIENCE*, *33*, 609–622.

696 Kirkby, J., J. Curtius, J. Almeida, E. Dunne, J. Duplissy, S. Ehrhart, A. Franchin,
697 S. Gagné, L. Ickes, A. Kürten, A. Kupc, A. Metzger, F. Riccobono, L. Rondo,
698 S. Schobesberger, G. Tsagkogeorgas, D. Wimmer, A. Amorim, F. Bianchi, M. Bre-
699 itenlechner, A. David, J. Dommen, A. Downard, M. Ehn, R. C. Flagan, S. Haider,
700 A. Hansel, D. Hauser, W. Jud, H. Junninen, F. Kreissl, A. Kvashin, A. Laakso-
701 nen, K. Lehtipalo, J. Lima, E. R. Lovejoy, V. Makhmutov, S. Mathot, J. Mikkilä,
702 P. Minginette, S. Mogo, T. Nieminen, A. Onnela, P. Pereira, T. Petäjä, R. Schnitzhofer,
703 J. H. Seinfeld, M. Sipilä, Y. Stozhkov, F. Stratmann, A. Tomé, J. Vanhanen, Y. Viisa-
704 nen, A. Vrtala, P. E. Wagner, H. Walther, E. Weingartner, H. Wex, P. M. Winkler, K. S.
705 Carslaw, D. R. Worsnop, U. Baltensperger, and M. Kulmala (2011), Role of sulphuric
706 acid, ammonia and galactic cosmic rays in atmospheric aerosol nucleation, *Nature*, *476*,
707 429–433, doi:10.1038/nature10343.

708 Kuang, C., P. H. McMurry, A. V. McCormick, and F. L. Eisele (2008), Dependence
709 of nucleation rates on sulfuric acid vapor concentration in diverse atmospheric
710 locations, *Journal of Geophysical Research (Atmospheres)*, *113*, D10209, doi:
711 10.1029/2007JD009253.

712 Kulmala, M., A. Laaksonen, and L. Pirjola (1998), Parametrizations for sulfuric acid/water
713 nucleation rates, *J. Geophys. Res.*, *103*, 8301–8308.

714 Kurtén, T., M. Noppel, H. Vehkamäki, M. Salonen, and M. Kulmala (2007), Quantum
715 chemical studies of hydrate formation of H_2SO_4 and HSO_4-, *Boreal Environment Re-*
716 *search*, *12*, 431–453.

717 Lamarque, J.-F., T. C. Bond, V. Eyring, C. Granier, A. Heil, Z. Klimont, D. Lee, C. Li-
718 ousse, A. Mieville, B. Owen, M. G. Schultz, D. Shindell, S. J. Smith, E. Stehfest,
719 J. Van Aardenne, O. R. Cooper, M. Kainuma, N. Mahowald, J. R. McConnell, V. Naik,
720 K. Riahi, and D. P. van Vuuren (2010), Historical (1850–2000) gridded anthropogenic
721 and biomass burning emissions of reactive gases and aerosols: methodology and appli-
722 cation, *Atmos. Chem. Phys.*, *10*(15), 7017–7039, doi:10.5194/acp-10-7017-2010.

723 Lee, S.-H., J. M. Reeves, J. C. Wilson, D. E. Hunton, A. A. Viggiano, T. M. Miller,
724 J. O. Ballenthin, and L. R. Lait (2003), Particle Formation by Ion Nucleation in
725 the Upper Troposphere and Lower Stratosphere, *Science*, *301*, 1886–1889, doi:
726 10.1126/science.1087236.

727 Lee, Y. H., J. R. Pierce, and P. J. Adams (2013), Representation of nucleation mode mi-
728 crophysics in a global aerosol model with sectional microphysics, *Geoscientific Model*
729 *Development*, *6*, 1221–1232, doi:10.5194/gmd-6-1221-2013.

730 Lehtinen, K. E. J., M. Dal Maso, M. Kulmala, and V.-M. Kerminen (2007), Estimating
731 nucleation rates from apparent particle formation rates and vice versa: Revised for-
732 mulation of the Kerminen-Kulmala equation, *JOURNAL OF AEROSOL SCIENCE*, *38*,
733 988–994.

734 Makkonen, R., A. Asmi, H. Korhonen, H. Kokkola, S. Järvenoja, P. Räisänen, K. E. J.
735 Lehtinen, A. Laaksonen, V.-M. Kerminen, H. Järvinen, U. Lohmann, R. Bennartz,
736 J. Feichter, and M. Kulmala (2009), Sensitivity of aerosol concentrations and cloud
737 properties to nucleation and secondary organic distribution in ECHAM5-HAM global
738 circulation model, *Atmospheric Chemistry & Physics*, *9*, 1747–1766.

739 McGouldrick, K., and O. B. Toon (2007), An investigation of possible causes of the holes
740 in the condensational Venus cloud using a microphysical cloud model with a radiative-
741 dynamical feedback, *Icarus*, *191*, 1–24, doi:10.1016/j.icarus.2007.04.007.

742 McGouldrick, K., O. B. Toon, and D. H. Grinspoon (2011), Sulfuric acid aerosols
743 in the atmospheres of the terrestrial planets, *Planet. Space Sci.*, *59*, 934–941, doi:
744 10.1016/j.pss.2010.05.020.

745 Merikanto, J., D. V. Spracklen, G. W. Mann, S. J. Pickering, and K. S. Carslaw (2009),
746 Impact of nucleation on global CCN, *Atmos. Chem. Phys.*, *9*, 8601–8616.

747 Merikanto, J., J. Duplissy, A. Määttänen, H. Henschel, N. M. Donahue, D. Brus,
748 S. Schobesberger, M. Kulmala, and H. Vehkamäki (2016), Effect of ions on sulfuric
749 acid-water binary particle formation I: Theory for kinetic and nucleation-type parti-
750 cle formation and atmospheric implications, *J. Geophys. Res.*, *121*, 1736–1751, doi:
751 10.1002/2015JD023539.

752 Modgil, M. S., S. Kumar, S. N. Tripathi, and E. R. Lovejoy (2005), A parameterization
753 of ion-induced nucleation of sulphuric acid and water for atmospheric conditions, *J.*
754 *Geophys. Res.*, *110*, D19,205.

Noppel, M., H. Vehkamäki, and M. Kulmala (2002), An improved model for hydrate formation in sulfuric-acid water nucleation, *J. Chem. Phys*, *116*, 218–228.

Ortega, I. K., O. Kupiainen, T. Kurtén, T. Olenius, O. Wilkman, M. J. McGrath, V. Loukonen, and H. Vehkamäki (2012), From quantum chemical formation free energies to evaporation rates, *Atmos. Chem. Phys.*, *12*, 225–235, doi:10.5194/acp-12-225-2012.

Pandis, S. N., L. M. Russell, and J. H. Seinfeld (1994), The relationship between dms flux and ccn concentration in remote marine regions, *J. Geophys. Res.*, *99*, 16,945–16,957.

Petäjä, T., R. L. Mauldin, III, E. Kosciuch, J. McGrath, T. Nieminen, P. Paasonen, M. Boy, A. Adamov, T. Kotiaho, and M. Kulmala (2009), Sulfuric acid and OH concentrations in a boreal forest site, *Atmos. Chem. Phys.*, *9*, 7435–7448.

Petäjä, T., M. Sipilä, P. Paasonen, T. Nieminen, T. Kurtén, I. K. Ortega, F. Stratmann, H. Vehkamäki, T. Berndt, and M. Kulmala (2011), Experimental Observation of Strongly Bound Dimers of Sulfuric Acid: Application to Nucleation in the Atmosphere, *Physical Review Letters*, *106*(22), 228302, doi:10.1103/PhysRevLett.106.228302.

Peter, T., and J.-U. Grooß (2012), *Stratospheric Ozone Depletion and Climate Change*, chap. 4: Polar stratospheric clouds and sulfate aerosol particles: microphysics, denitrification and heterogeneous chemistry., pp. 108–144, The Royal Society of Chemistry.

Pitari, G., E. Mancini, V. Rizi, and D. T. Shindel (2002), Impact of future climate and emission changes on stratospheric aerosols and ozone, *J. Atmos. Sci*, *59*, 414–440.

Raes, F. (1995), Entrainment of free tropospheric aerosols as a regulating mechanism for cloud condensation nuclei in the remote marine boundary layer, *J. Geophys. Res.*, *100*, 2893–2903.

Sawamura, P., J. P. Vernier, J. E. Barnes, T. A. Berkoff, E. J. Welton, L. Alados-Arboledas, F. Navas-Guzmán, G. Pappalardo, L. Mona, F. Madonna, D. Lange, M. Sicard, S. Godin-Beekmann, G. Payen, Z. Wang, S. Hu, S. N. Tripathi, C. Cordoba-Jabonero, and R. M. Hoff (2012), Stratospheric AOD after the 2011 eruption of Nabro volcano measured by lidars over the Northern Hemisphere, *Environ. Res. Lett.*, *7*(3), 034,013, doi:10.1088/1748-9326/7/3/034013.

Seinfeld, J. H., and S. N. Pandis (1998), *Atmospheric Chemistry and Physics: From Air Pollution to Climate Change*, John Wiley & Sons, New York.

Sihto, S.-L., M. Kulmala, V.-M. Kerminen, M. Dal Maso, T. Petäjä, I. Riipinen, H. Korhonen, F. Arnold, R. Janson, M. Boy, A. Laaksonen, and K. E. J. Lehtinen (2006),

Atmospheric sulphuric acid and aerosol formation: implications from atmospheric measurements for nucleation and early growth mechanisms, *Atmos. Chem. Phys.*, *6*, 4079–4091.

Sipilä, M., T. Berndt, T. Petäjä, D. Brus, J. Vanhanen, F. Stratmann, J. Patokoski, R. L. Mauldin, A.-P. Hyvärinen, H. Lihavainen, and M. Kulmala (2010), The Role of Sulfuric Acid in Atmospheric Nucleation, *Science*, *327*, 1243–, doi:10.1126/science.1180315.

Solomon, S., J. S. Daniel, R. R. Neely, J.-P. Vernier, E. G. Dutton, and L. W. Thomason (2011), The Persistently Variable Background Stratospheric Aerosol Layer and Global Climate Change, *Science*, *333*, 866–, doi:10.1126/science.1206027.

Spracklen, D. V., K. S. Carslaw, M. Kulmala, V.-M. Kerminen, S.-L. Sihto, I. Riipinen, J. Merikanto, G. W. Mann, M. P. Chipperfield, A. Wiedensohler, W. Birmili, and H. Lihavainen (2008), Contribution of particle formation to global cloud condensation nuclei concentrations, *Geophys. Res. Lett.*, *35*, L06808, doi:10.1029/2007GL033038.

Stier, P., J. Feichter, S. Kinne, S. Kloster, E. Vignati, J. Wilson, L. Ganzeveld, I. Tegen, M. Werner, Y. Balkanski, M. Schulz, O. Boucher, A. Minikin, and A. Petzold (2005), The aerosol-climate model ECHAM5-HAM, *Atmos. Chem. Phys.*, *5*, 1125–1156.

Trinkaus, H. (1983), Theory of the nucleation of multicomponent precipitates, *Phys. Rev. B.*, *27*, 7372–7378.

Vehkamäki, H. (2006), *Classical Nucleation Theory in Multicomponent Systems*, Springer, Berlin Heidelberg.

Vehkamäki, H., M. Kulmala, I. Napari, K. E. J. Lehtinen, C. Timmreck, M. Noppel, and A. Laaksonen (2002), An improved parameterization for sulfuric acid/water nucleation rates for tropospheric and stratospheric conditions, *J. Geophys. Res.*, *107*, 10.1029/2002JD00.

Vehkamäki, H., M. Kulmala, and K. E. J. Lehtinen (2003), Modelling binary homogeneous nucleation of water-sulfuric acid vapours: parameterisation for high temperature emissions, *Environ. Sci. Technol.*, *37*, 3392–3398.

Vernier, J.-P., L. W. Thomason, J.-P. Pommereau, A. Bourassa, J. Pelon, A. Garnier, A. Hauchecorne, L. Blanot, C. Trepte, D. Degenstein, and F. Vargas (2011), Major influence of tropical volcanic eruptions on the stratospheric aerosol layer during the last decade, *Geophys. Res. Lett.*, *38*, L12807, doi:10.1029/2011GL047563.

Weber, R. J., J. Marti, P. H. McMurry, F. Eisele, D. J. Tanner, and A. Jefferson (1996), Measured atmospheric new particle formation rates: implications for nucleation mecha-

nisms, *Chem. Eng. Comm*, *151*, 53–64.

Wexler, A. S., F. W. Lurmann, and J. H. Seinfeld (1994), Modelling urban and regional aerosols:i. modeling development, *Atm. Environ.*, *28*, 531–546.

Wilemski, G., and B. E. Wyslouzil (1995), Binary nucleation kinetics. I. Self-consistent size distribution, *J. Chem. Phys.*, *103*, 1127–1136.

Young, A. T. (1983), Venus cloud microphysics, *Icarus*, *56*, 568–577, doi:10.1016/0019-1035(83)90174-4.

Yu, F. (2008), Updated H_2SO_4-H_2O binary homogeneous nucleation look-up tables, *Journal of Geophysical Research (Atmospheres)*, *113*, D24201, doi:10.1029/2008JD010527.

Yu, F. (2010), Ion-mediated nucleation in the atmosphere: Key controlling parameters, implications, and look-up table, *J. Geophys. Res.*, *115*, D03206, doi:10.1029/2009JD012630.

Yu, F., G. Luo, T. S. Bates, B. Anderson, A. Clarke, V. Kapustin, R. M. Yantosca, Y. Wang, and S. Wu (2010), Spatial distributions of particle number concentrations in the global troposphere: Simulations, observations, and implications for nucleation mechanisms, *Journal of Geophysical Research: Atmospheres*, *115*(D17), n/a–n/a, doi:10.1029/2009JD013473, d17205.

Zhang, K., D. O'Donnell, J. Kazil, P. Stier, S. Kinne, U. Lohmann, S. Ferrachat, B. Croft, J. Quaas, H. Wan, S. Rast, and J. Feichter (2012), The global aerosol-climate model ECHAM-HAM, version 2: sensitivity to improvements in process representations, *Atmos. Chem. Phys.*, *12*, 8911–8949, doi:10.5194/acp-12-8911-2012.

Zhang, Y., P. H. McMurry, F. Yu, and M. Z. Jacobson (2010), A comparative study of nucleation parameterizations: 1. Examination and evaluation of the formulations, *Journal of Geophysical Research (Atmospheres)*, *115*, D20212, doi:10.1029/2010JD014150.

Zhao, J., F. L. Eisele, M. Titcombe, C. Kuang, and P. H. McMurry (2010), Chemical ionization mass spectrometric measurements of atmospheric neutral clusters using the cluster-cims, *J. Geophys. Res.*, *115*, D08,205, doi:10.1029/2009JD012606.